Geochemistry Geophysics Geosystems G3
AN ELECTRONIC JOURNAL OF THE EARTH SCIENCES
Published by AGU and the Geochemical Society

Article
Volume 10, Number 4
25 April 2009
Q04014, doi:10.1029/2008GC002281
ISSN: 1525-2027

Mantle source variations beneath the Eastern Lau Spreading Center and the nature of subduction components in the Lau basin–Tonga arc system

S. Escrig and A. Bézos
Department of Earth and Planetary Sciences, Harvard University, 20 Oxford Street, Cambridge, Massachusetts 02138, USA (escrig@eps.harvard.edu)

S. L. Goldstein
Lamont-Doherty Earth Observatory, Earth Institute at Columbia University, 61 Route 9W, Palisades, New York 10964, USA

Department of Earth and Environmental Sciences, Columbia University, 61 Route 9W, Palisades, New York 10964, USA

C. H. Langmuir
Department of Earth and Planetary Sciences, Harvard University, 20 Oxford Street, Cambridge, Massachusetts 02138, USA

P. J. Michael
Department of Geosciences, University of Tulsa, 800 South Tucker Avenue, Tulsa, Oklahoma 74104, USA

[1] New high-density sampling of the Eastern Lau Spreading Center provides constraints on the processes that affect the mantle wedge beneath a back-arc environment, including the effect of the subduction input on basalt petrogenesis and the change in subduction input with distance from the Tonga arc. We obtained trace element and Pb-Sr-Nd isotopic compositions of 64 samples distributed between 20.2°S and 22.3°S with an average spacing of ~3.6 km. The trace element and isotope variations do not vary simply with distance from the arc and reflect variations in the mantle wedge composition and the presence of multiple components in the subduction input. The mantle wedge composition varies form north to south, owing to the southward migration of Indian-like mantle, progressively replacing the initially Pacific-like mantle wedge. The mantle wedge compositions also require an enriched mid-ocean ridge basalt–like trace element enrichment that has little effect on isotope ratios, suggesting recent low-degree melt enrichment events. The composition of the subduction input added to the mantle wedge is geographically variable and mirrors the changes observed in the Tonga arc island lavas. The combination of the back-arc and arc data allows identification of several components contributing to the subduction input. These are a fluid derived from the altered oceanic crust with a possible sedimentary contribution, a pelagic sediment partial melt, and, in the southern Lau basin, a volcaniclastic sediment partial melt. While on a regional scale, there is a rough decrease in subduction influence with the distance from the arc, on smaller scales, the distribution of the subduction input reflects different mechanisms of the addition of the subduction input to a variable mantle wedge.

Components: 18,974 words, 17 figures, 3 tables.

Keywords: back-arc basin; back-arc basalt; subduction component; mantle wedge; enrichment processes.

Index Terms: 1040 Geochemistry: Radiogenic isotope geochemistry; 1031 Geochemistry: Subduction zone processes (3060, 3613, 8170, 8413); 1038 Geochemistry: Mantle processes (3621).

Received 15 October 2008; **Revised** 12 February 2009; **Accepted** 25 February 2009; **Published** 25 April 2009.

Escrig, S., A. Bézos, S. L. Goldstein, C. H. Langmuir, and P. J. Michael (2009), Mantle source variations beneath the Eastern Lau Spreading Center and the nature of subduction components in the Lau basin–Tonga arc system, *Geochem. Geophys. Geosyst.*, *10*, Q04014, doi:10.1029/2008GC002281.

1. Introduction

[2] Back-arc spreading centers (BASC) represent a small but significant fraction of the global ocean ridge system, and are an integral part of many subduction zones. Back-arc basin basalts (BABB) have large ion lithophile elements (LILE) and water contents intermediate to those of typical MORB and spatially related arc basalts [*Taylor and Martinez*, 2003; *Kelley et al.*, 2006; *Langmuir et al.*, 2006, and references therein]. BABB have also been used to show spatial gradients in the mantle composition beneath back-arc basins [*Pearce et al.*, 2005, 2007]. BASC combine the relative simplicity of a ridge environment, where magmatism is less encumbered by assimilation and contamination, with moderate subduction-related contributions compared to arc volcanism. BASC provide important perspectives on processes that occur in a subduction environment, including the effect of fluids on basalt petrogenesis, the pathways of the subduction input, and mantle enrichment. Moreover, because the mantle wedge volume is limited by the slab boundary, it is possible that BABB production depletes the wedge that is available for arc front generation, and vice versa. In these ways, integrated knowledge of back-arc and arc front volcanism can give us a much better knowledge of the processes and dynamics of the entire subduction system.

[3] The Lau basin, located behind the Tonga arc, contains several spreading centers distributed over a basin 600 km long and up to 500 km wide (Figure 1). Previous studies of on-axis samples [*Sunkel*, 1990; *Falloon et al.*, 1992; *Volpe et al.*, 1988; *Loock*, 1992; *Pearce et al.*, 1994; *Peate et al.*, 2001; *Hergt and Woodhead*, 2007; *Pearce et al.*, 2007], from ODP drilling (Leg 135, Sites 834 to 839 [*Ewart et al.*, 1994a, 1994b; *Hawkins and Allan*, 1994; *Hergt and Farley*, 1994; *Hergt and Hawkesworth*, 1994; *Ewart et al.*, 1998]) and arc islands [*Pearce et al.*, 1995; *Regelous et al.*, 1997; *Turner et al.*, 1997; *Turner and Hawkesworth*, 1997; *Wendt et al.*, 1997; *Ewart et al.*, 1998; *Turner and Hawkesworth*, 1998; *Pearce et al.*, 2007] have revealed geochemical variations in the mantle wedge composition and in the subduction-related components, as well as possible contribution of enriched material from the Louisville Seamount Chain (LSC) and the Samoan hot spot. Samples from ODP Leg 135 (Sites 834 to 839) indicate that the mantle wedge composition has changed in the past because of the propagation southward of an Indian-like mantle replacing Pacific-like mantle [*Ewart et al.*, 1994b; *Hergt and Farley*, 1994; *Hergt and Hawkesworth*, 1994; *Ewart et al.*, 1998]. A similar transition is also displayed by modern eruptives from the Eastern Lau Spreading Center (ELSC) [*Peate et al.*, 2001]. Recently, on the basis of Nd-Hf isotopes in arc and back-arc samples from the Lau basin–Fiji region, *Pearce et al.* [2007] have confirmed the transition between Pacific and Indian-like mantle regions in the southern Lau basin and related the Indian-like signature to the propagation southward of a Pacific enriched "SOPITA" mantle (South Pacific Isotopic and Thermal Anomaly [*Staudigel et al.*, 1991]) following the collision of the Ontong-Java Plateau with the Vitiaz Trench 12 Ma ago. They also revealed significant isotopic variation within the two mantle domains, which they attributed to progressive depletion by melt extraction of the mantle as it migrates southward. The precise location and the nature of the transition between the Pacific and Indian-like mantle regions must lie somewhere between the Central Lau Spreading Center (CLSC, north of ~18°S) and Valu Fa (22°S) but has not been precisely known because sampling has been too sparse until now [*Pearce et al.*, 1994; *Peate et al.*, 2001; *Pearce et al.*, 2007].

[4] The chemical signature of BAB lavas worldwide is variable and has multiple origins. One type of enrichment is associated with an arc-like component, enriched in fluid mobile elements and large ion lithophile elements (LILE) such as Rb, Ba, Th, K, but not in high field strength elements (HFSE) such as Nb, Ta, Hf, Zr. In some locations such as the Mariana and East Scotia back-arc basins

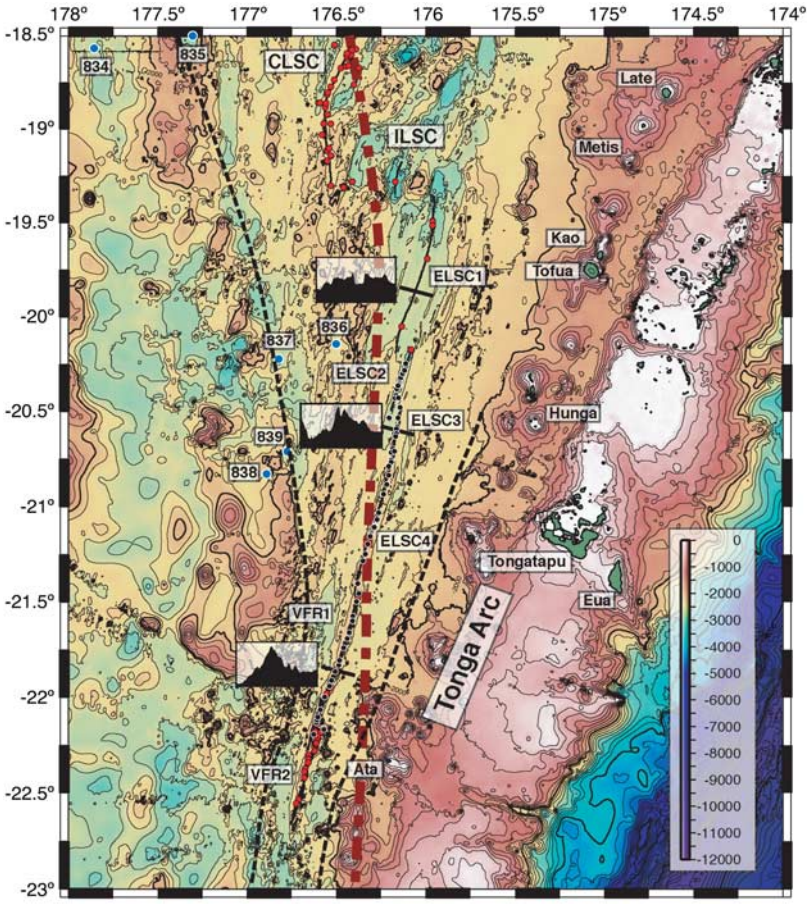

Figure 1. Bathymetric map showing sample locations (black circles, samples reported in this study (cruise KM0417); red circles, CLSC, ILSC, and other ELSC samples; and blue circles, ODP site locations (see Appendix C for sources of locations)). Three cross sections illustrate the change in ridge morphology along the Eastern Lau Spreading Center. The black dashed lines represent the limit between old and young crust [*Martinez and Taylor*, 2002], and the thick red dashed line represents the projected location of the subducted Louisville Seamounts Chain [*Regelous et al.*, 1997].

(Figure 2), the enrichment in fluid mobile elements (responsible for the high Ba/Nb) is coupled with an enrichment in melt mobile (incompatible) elements (responsible for the high La/Sm). In contrast, the arc-like component in the Lau basin displays minimal enrichment in melt mobile elements. Another cause of variability in BAB lavas is the degree of depletion or enrichment of the mantle wedge preceding the addition of the arc-like component. Evidence for enriched mantle (similar to a enriched mid-oceanic ridge basalt (E-MORB) mantle source) has been found in all back-arc basins [*Danyushevsky et al.*, 1993; *Sinton et al.*, 2003; *Pearce et al.*, 2005; *Langmuir et al.*, 2006]. *Langmuir et al.* [2006] have attributed this enrichment in incompatible elements to recent addition of low-degree melts to the mantle wedge, as proposed by *Donnelly et al.* [2004] for the E-MORB source.

[5] Most studies of the subduction input to the Tonga-Lau subduction zone have dealt with the Tonga arc islands [*Regelous et al.*, 1997; *Turner et al.*, 1997; *Ewart et al.*, 1998]. Data showing ^{238}U excesses over ^{230}Th [*Turner et al.*, 1997; *Peate et al.*, 2001] and strong enrichments of LILE/HFSE [*Turner et al.*, 1997; *Ewart et al.*, 1998; *Peate et al.*, 2001; *Hergt and Woodhead*, 2007] demonstrate the importance of recent addition of hydrous fluid to the mantle wedge. This suggests that the fluid mobile and incompatible element budget of Tonga arc lavas is controlled by mixing between a fluid from altered ocean crust (AOC) and either a partial melt [*Regelous et al.*, 1997; *Turner et al.*, 1997; *Peate et al.*, 2001] or a fluid [*Hergt and Woodhead*, 2007] derived from pelagic sediments. Because of the wide spacing of the arc islands and the limited sampling along the ELSC, none of the earlier studies of Lau basin volcanic products discussed

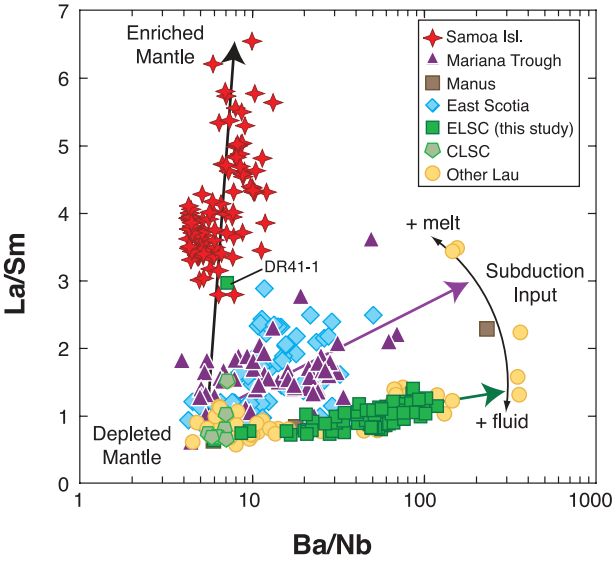

Figure 2. La/Sm versus Ba/Nb modified from *Langmuir et al.* [2006] (see Appendix C for data sources). Most of the on-axis samples from ELSC plot on a shallow trend pointing toward high Ba/Nb and moderate La/Sm, consistent with little preconditioning of the mantle wedge by low-degree melts (as illustrated by Samoan lavas). Only sample DR41-1 displays a trace element composition comparable to the Samoan lavas. The samples labeled "Other Lau" correspond to off-axis samples. For comparison, also shown are data from other back-arc basins. East Scotia and Mariana point toward a subduction component with higher La/Sm than Lau or Manus reflecting a higher melt contribution.

in detail the compositional variability of the subduction input and its relationship with the distance from the arc front.

[6] Our systematic sampling of the ELSC provides a new opportunity to examine the nature of the enrichment processes and the mantle wedge evolution in one of the best developed arc-back-arc systems, the Tonga arc and Lau basin. In this paper we report new isotopic and trace element data from the ELSC, as well as new Pb isotope data for the Tonga arc, which we compile with published data. We use the data to address the following questions. Is there systematic geochemical variability along the ELSC with the distance from the arc as proposed by *Pearce et al.* [1994]? Are the trace element and isotope variations in BABB due to changes in the amount of a subduction component or are they also related to compositional changes of the subduction component itself? If the composition changes, does it change with the distance from the arc and does it relate to Tonga arc variation?

[7] Once we understand the compositional and spatial variations of the subduction component(s), we can address the origin of the variation in the mantle wedge that existed prior to the addition of the subduction component(s). We pay particular attention to immobile trace elements and radiogenic isotopes to determine the nature, location and sharpness of the boundary between Pacific-like and Indian-like mantles in the wedge. The new data also allow us to define relationships between mantle source composition, ridge segmentation, along-axis bathymetry and the ridge morphology that help us to understand mantle dynamics and melting beneath back-arc spreading centers.

2. Geological Setting

[8] The Eastern Lau Spreading Center (ELSC) and Valu Fa Ridge (VFR) occupy a single first-order ridge segment in the southern Lau basin, and are divided into smaller segments by multiple small offsets (Figure 1). The ELSC includes four segments (numbered ELSC1 to ELSC4 from north to south), and the Valu Fa ridge includes two segments (VFR1 and VFR2, from north to south). Most of our samples from Valu Fa are located along VFR1, extending southward from segment ELSC4. At every offset, the northernmost segment is shifted toward the west, farther away from the arc. The distance of each segment from the Tonga Arc front increases progressively from 40 km at the southern extremity of the Valu Fa Ridge to 100 km in the northern extremity of ELSC. A small segment, the Intermediate Lau spreading center (ILSC), separates the ELSC from the Central Lau Spreading Center (CLSC), located even farther from the volcanic front of the arc, about 50 km to the northwest.

[9] The current phase of seafloor spreading started about 3–4 Ma ago and has propagated rapidly southward [*Karig*, 1970; *Taylor et al.*, 1996]. The spreading rate decreases southward from 85 to 92 mm/a along the CLSC to 40 mm/a at the southern end of the ELSC [*Taylor and Martinez*, 2003] as the subduction rate changes from 160 mm/a in the north to 80 mm/a in the south [*Bevis et al.*, 1995]. A transition in ridge morphology associated with a substantial decrease of depth, from 2700 m to 2100 m, occurs in the middle of ELSC3, a 30-km-long segment. The northern ELSC segments are characterized by an axial depression (inset in Figure 1) and show relatively constant bathymetric depths of 2700 m, except for the northern extremity where the depth reaches 3000 m. From the middle of

Table 1. Pb, Sr, and Nd Isotope Ratios and Trace Element Contents[a]

	Group	Longitude (°E)	Latitude (°N)	Depth (m)	Mg #	$^{206}Pb/^{204}Pb$	$^{207}Pb/^{204}Pb$	$^{208}Pb/^{204}Pb$	$^{87}Sr/^{86}Sr$	$^{143}Nd/^{144}Nd$	Sr (ppm)	La (ppm)	Ce (ppm)	Nd (ppm)	Sm (ppm)	Nb (ppm)	Ba (ppm)	Pb (ppm)	Th (ppm)	U (ppm)
ELSC II																				
KM0417 RC031	N	−176.11	−20.25	2778	0.59	18.230	15.512	38.041	0.703195	0.513051	79	1.76	5.91	6.19	2.26	1.09	10.4	0.45	0.098	0.031
KM0417 RC107	N	−176.12	−20.28	2840	0.61	18.130	15.502	37.949	0.703161	0.513043	79	1.61	5.52	5.84	2.15	0.78	6.7	0.38	0.084	0.02
KM0417 RC075	N	−176.13	−20.3	1667	0.59	18.294	15.519	38.077	0.703200	0.513041	88	1.61	5.6	5.92	2.21	0.65	10.8	0.45	0.075	0.028
KM0417 DR53-1	N	−176.13	−20.31	2738	0.59	18.331	15.523	38.080	0.703180	0.513063	86	1.67	5.64	5.9	2.12	0.75	15	0.46	0.086	0.033
KM0417 DR11-2	N	−176.14	−20.32	2731	0.59	18.332	15.524	38.082	0.703180	0.513051	86	1.71	5.63	5.85	2.13	0.74	15.2	0.39	0.088	0.033
KM0417 DR11-2 duplicate	N					18.329	15.523	38.079	0.703177	0.513049										
KM0417 RC026	N	−176.14	−20.32	2722	0.53	18.361	15.506	38.034	0.703196	0.513076	101	1.91	5.98	5.95	2.07	1.14	25.5	0.74	0.127	0.05
KM0417 RC024	N	−176.14	−20.33	2721	0.59	18.333	15.528	38.091	0.703211	0.513067	89	1.63	5.53	5.81	2.11	0.73	15.1	0.53	0.083	0.032
KM0417 RC028	N	−176.15	−20.35	2678	0.63	18.144	15.517	37.990	0.703167	0.513064	73	1.22	4.31	4.78	1.88	0.6	3.6	0.26	0.052	0.017
KM0417 RC028 duplicate	N									0.513059										
KM0417 RC076	N	−176.15	−20.36	2700	0.6	18.400	15.532	38.144	0.703207	0.513043	103	1.61	5.49	5.7	2.05	0.59	17.1	0.48	0.083	0.035
KM0417 RC077	N	−176.16	−20.36	2713	0.6	18.340	15.522	38.081	0.703190	0.513078	88	1.68	5.66	5.88	2.11	0.76	16.7	0.52	0.089	0.036
KM0417 DR10-1	N	−176.16	−20.38	2686	0.62	18.404	15.537	38.169	0.703186	0.513031	119	1.49	5.18	5.7	2.01	0.52	14.6	0.47	0.071	0.03
KM0417 RC098	N	−176.17	−20.42	2676	0.66	18.392	15.523	38.101	0.703194	0.513065	95	1.21	4.17	4.4	1.59	0.43	14.5	0.47	0.063	0.027
KM0417 RC099	N	−176.17	−20.43	2567	0.64	18.179	15.517	38.049	0.703261	0.512983	83	1.35	4.79	5.18	1.91	0.65	4.5	0.38	0.063	0.018
KM0417 RC099 duplicate	N					18.172	15.517	38.038	0.703259	0.513011										
KM0417 DR41-1	N	−176.21	−20.53	2488	0.67	18.273	15.508	38.043	0.703042	0.513018	193	9.36	20.75	12.64	3.15	14.81	105.1	0.92	1.068	0.286
ELSC III																				
KM0417 RC106	N	−176.15	−20.43	2501	0.57	18.286	15.519	38.051	0.703261	0.513042	88	1.8	6.13	6.43	2.31	0.97	15.2	0.52	0.093	0.033
KM0417 RC104	N	−176.14	−20.48	2516	0.64	18.315	15.529	38.097	0.703193	0.513055	90	1.34	4.53	4.87	1.81	0.6	12.3	0.42	0.074	0.026
KM0417 DR40-1	N	−176.15	−20.53	2535	0.56	18.402	15.531	38.137	0.703213	0.513059	95	1.61	5.4	5.71	2.06	0.86	24.7	0.51	0.099	0.037
KM0417 RC032	N	−176.16	−20.58	2549	0.5	18.394	15.512	38.029	0.702836	0.513058	280	2.63	8.12	7.77	2.56	1.07	21.8	0.96	0.146	0.061
KM0417 RC032 duplicate	N-C					18.388	15.511	38.004	0.702781	0.513039										
KM0417 RC080	N-C	−176.16	−20.59	2460	0.6	18.406	15.529	38.106	0.703059	0.513058	131	1.68	5.36	5.37	1.86	0.67	20.4	0.57	0.097	0.04
KM0417 DR42-1	C	−176.18	−20.62	2403	0.52	18.487	15.544	38.188	0.703217	0.513059	118	1.86	5.91	5.99	2.11	0.85	40.4	0.69	0.122	0.053
KM0417 RC081	C	−176.16	−20.62	2490	0.57	18.524	15.550	38.237	0.703274	0.513053	107	1.56	4.77	4.74	1.66	0.63	37.7	0.74	0.106	0.053
KM0417 RC087	C	−176.17	−20.63	2417	0.58	18.505	15.539	38.192	0.703277	0.513049	105	1.51	4.64	4.67	1.65	0.65	36.8	0.69	0.104	0.048
KM0417 RC084	C	−176.19	−20.7	2182	0.39	18.458	15.539	38.163	0.703225	0.513056	118	2.8	8.71	8.66	2.99	1.5	50.3	0.92	0.186	0.076
KM0417 RC085	C	−176.19	−20.72	2233	0.44	18.464	15.536	38.161	0.703233	0.513061	122	2.51	7.89	7.86	2.8	1.22	49.8	0.92	0.162	0.07
ELSC IV																				
KM0417 RC088	C	−176.18	−20.71	2286	0.54	18.481	15.539	38.167	0.703223	0.513072	104	1.58	5.12	5.33	1.95	0.69	38.4	0.67	0.101	0.046
KM0417 DR51-1	C	−176.19	−20.76	2032	0.34	18.466	15.539	38.185	0.703259	0.513064	128	2.75	9.07	9.08	3.1	1.27	72.1	1.07	0.159	0.074
KM0417 DR50-1	C	−176.19	−20.77	2132	0.38	18.490	15.537	38.186	0.703265	0.513063	127	2.65	8.71	8.76	3.04	1.21	71.6	1.03	0.15	0.076
KM0417 DR12-1	C	−176.21	−20.79	2226	0.46	18.475	15.540	38.166	0.703248	0.513057	115	1.81	5.79	6.05	2.18	0.82	40.4	0.71	0.112	0.053
KM0417 RC038	C	−176.21	−20.83	2200	0.37	18.501	15.536	38.186	0.703282	0.513051	128	2.52	8.27	8.33	2.83	1.14	70.6	1.04	0.149	0.07
KM0417 RC037	C	−176.22	−20.88	2225	0.51	18.460	15.525	38.126	0.703191	0.513065	139	1.95	6.15	6.22	2.15	0.74	48.5	1.08	0.112	0.055
KM0417 RC036	C	−176.24	−20.93	2266	0.41	18.426	15.535	38.132	0.703008	0.513053	153	2.32	7.33	7.27	2.46	0.94	42.5	0.81	0.126	0.054

Table 1. (continued)

	Group	Longitude (°E)	Latitude (°N)	Depth (m)	Mg #	$^{206}Pb/^{204}Pb$	$^{207}Pb/^{204}Pb$	$^{208}Pb/^{204}Pb$	$^{87}Sr/^{86}Sr$	$^{143}Nd/^{144}Nd$	Sr (ppm)	La (ppm)	Ce (ppm)	Nd (ppm)	Sm (ppm)	Nb (ppm)	Ba (ppm)	Pb (ppm)	Th (ppm)	U (ppm)
KM0417 RC036 duplicate	C					18.423	15.533	38.120	0.703029											
KM0417 RC045	C	−176.26	−21.03	2322	0.34	18.459	15.529	38.154	0.703260	0.513076	116	2.57	5.52	8.73	3.09	1.09	56.1	0.86	0.14	0.062
KM0417 RC043	C	−176.27	−21.07	2425	0.43	18.461	15.534	38.169	0.703240	0.513066	120	2.93	8.84	8.38	2.94	1.71	51.7	0.86	0.21	0.079
KM0417 DR14-1	C	−176.28	−21.09	2317	0.38	18.463	15.537	38.184	0.703247	0.513067	114	2.66	8.96	9.14	3.22	1.14	55	0.93	0.141	0.063
KM0417 DR13-1	C	−176.29	−21.1	2160	0.3	18.467	15.538	38.187	0.703258	0.513060	119	2.54	8.43	8.69	3.03	1.11	54.4	0.92	0.139	0.061
KM0417 DR13-1 duplicate	C					18.466	15.539	38.185	0.703246	0.513064										
KM0417 RC040	C	−176.29	−21.1	2307	0.32	18.459	15.536	38.171	0.703235	0.513068	119	2.76	9.18	9.4	3.32	1.18	58.3	0.91	0.148	0.066
KM0417 RC039	C-S	−176.29	−21.11	2268	0.32	18.504	15.536	38.247	0.703203	0.513070	145	3.96	12.65	12.19	4.11	1.62	61	1.26	0.245	0.099
KM0417 RC050	C-S	−176.31	−21.14	2301	0.34	18.491	15.538	38.201	0.703153	0.513047	131	3.49	10.17	9.59	3.31	1.83	62.4	0.97	0.26	0.101
KM0417 RC049	C-S	−176.31	−21.15	2290	0.34	18.366	15.524	38.087	0.703087	0.513058	117	3.26	10.49	10.5	3.66	1.71	44.9	0.92	0.187	0.069
KM0417 RC048	C-S	−176.31	−21.16	2267	0.38	18.534	15.559	38.279	0.703251	0.513055	135	3.36	10.24	9.61	3.36	1.5	142	1.59	0.241	0.112
KM0417 RC047	C-S	−176.33	−21.2	2219	0.2	18.502	15.527	38.197	0.703171	0.513052	140	4.91	14.45	13.68	4.59	1.87	75.7	1.47	0.352	0.147
KM0417 RC046	S	−176.34	−21.25	2205	0.35	18.566	15.547	38.285	0.703211	0.513059	144	4.41	12.95	11.84	3.85	1.59	94.6	1.21	0.343	0.138
KM0417 RC046 duplicate	S					18.562	15.541	38.278	0.703198	0.513045										
KM0417 RC074	S	−176.35	−21.29	2060	0.34	18.566	15.537	38.263	0.703173	0.513059	150	4.67	13.72	12.42	3.95	1.83	76.2	1.17	0.366	0.142
KM0417 DR36-3	S	−176.38	−21.4	1970	0.43	18.534	15.542	38.242	0.703161	0.513065	128	3.03	9.03	8.56	2.94	1.06	54.4	0.93	0.211	0.08
VFR I																				
KM0417 RC073	S	−176.38	−21.46	1835	0.62	18.626	15.539	38.278	0.703246	0.513050	119	1.62	4.44	4.05	1.4	0.4	47	0.62	0.142	0.057
KM0417 RC052	S	−176.39	−21.5	1837	0.37	18.642	15.549	38.338	0.703211	0.513035	168	4.54	12.46	10.64	3.38	1.16	98	1.28	0.383	0.162
KM0417 DR34-2	S	−176.41	−21.58	1900	0.34	18.544	15.531	38.230	0.703152	0.513068	147	4.65	14.14	12.91	4.26	1.64	75.3	1.24	0.357	0.145
KM0417 DR34-2 duplicate	S					18.551	15.538	38.249	0.703148	0.513058										
KM0417 RC072	S	−176.41	−21.6	1880	0.36	18.635	15.548	38.321	0.703263	0.513067	155	4.98	14.02	12.54	4.08	1.33	104.2	1.31	0.424	0.178
KM0417 RC053	S	−176.43	−21.66	1798	0.61	18.623	15.551	38.301	0.703294	0.513081	114	1.61	4.95	4.82	1.67	0.49	36.8	0.64	0.119	0.05
KM0417 RC071	S	−176.44	−21.69	1816	0.34	18.613	15.544	38.302	0.703241	0.513072	148	4.88	13.94	12.5	4.13	1.37	100.6	1.31	0.407	0.169
KM0417 RC070	S	−176.46	−21.74	1901	0.33	18.597	15.543	38.279	0.703247	0.513078	144	3.44	10.08	9.2	3.16	1.01	70.8	1.25	0.262	0.113
KM0417 RC066	S	−176.48	−21.81	1752	0.33	18.569	15.536	38.267	0.703187	0.513037	158	4.07	11.71	10.77	3.6	1.24	67.5	1.06	0.311	0.126
KM0417 RC054	S	−176.49	−21.83	1972	0.36	18.535	15.523	38.216	0.703142	0.513052	153	3.7	10.84	10.12	3.39	1.18	58.9	1.17	0.274	0.11
KM0417 RC054	S	−176.49	−21.83	1972		18.551	15.538	38.262	0.703139	0.513053										
KM0417 RC067	S	−176.51	−21.87	1753	0.44	18.564	15.537	38.248	0.703201	0.513049	137	2.85	8.48	7.98	2.74	0.88	56.5	0.89	0.213	0.092
KM0417 RC067 duplicate	S								0.703200	0.513049										
KM0417 RC068	S	−176.53	−21.91	1922	0.16	18.653	15.547	38.336	0.703272	0.513061	147	8.1	22.19	17.94	5.75	2.03	173	2.31	0.764	0.33
KM0417 RC069	S	−176.54	−21.94	1755	0.38	18.620	15.542	38.300	0.703269	0.513069	145	4.05	11.52	10.18	3.38	1.07	88.9	1.24	0.344	0.149
KM0417 RC069 duplicate	S								0.703229	0.513061										
KM0417 RC060	S	−176.57	−22	1886	0.36	18.573	15.543	38.282	0.703190	0.513050	154	3.9	11.37	10.53	3.51	1.18	66	1.11	0.307	0.13
KM0417 RC061	S	−176.59	−22.07	1751	0.4	18.593	15.544	38.286	0.703236	0.513061	141	2.83	8.38	7.9	2.7	0.82	62	1.15	0.213	0.091
KM0417 RC059	S	−176.6	−22.1	1657	0.41	18.605	15.544	38.289	0.703234	0.513060	145	2.36	6.97	6.56	2.23	0.66	58.4	0.93	0.186	0.08

Table 1. (continued)

	Group	Longitude (°E)	Latitude (°N)	Depth (m)	Mg #	$^{206}Pb/^{204}Pb$	$^{207}Pb/^{204}Pb$	$^{208}Pb/^{204}Pb$	$^{87}Sr/^{86}Sr$	$^{143}Nd/^{144}Nd$	Sr (ppm)	La (ppm)	Ce (ppm)	Nd (ppm)	Sm (ppm)	Nb (ppm)	Ba (ppm)	Pb (ppm)	Th (ppm)	U (ppm)
KM0417 RC058	S	−176.61	−22.12	1588	0.5	18.615	15.546	38.293	0.703238	0.513055	144	2.01	5.97	5.63	1.94	0.54	54.3	0.8	0.158	0.069
KM0417 RC057	S	−176.61	−22.13	1654	0.55	18.643	15.544	38.310	0.703238	0.513070	160	3.09	8.41	7.36	2.43	0.74	75	0.95	0.279	0.121
KM0417 DR21-4	S	−176.57	−22.17	2054	0.36	18.662	15.551	38.352	0.703298	0.513054	163	4.07	11.12	9.82	3.24	1.01	89.8	1.16	0.358	0.157
KM0417 DR34-1	S	−176.57	−22.17	2054		18.542	15.532	38.228	0.703145	0.513072										
KM0417 DR16-1	S	−176.63	−22.2	1755	0.32	18.662	15.548	38.342	0.703324	0.513054	174	4.86	13.71	12.03	3.88	1.22	112.3	1.36	0.453	0.192
KM0417 DR16-1 duplicate	S					18.657	15.546	38.339	0.703312	0.513058										
Tonga arc islands																				
482-8-1		Ata				18.714	15.563	38.357	*0.703420*		*264*	*0.31*			*124*	*2.79*	*6.8*	*5.79*	*1.55*	*1.6*
482-8-4		Ata				18.753	15.563	38.396	*0.703340*	*0.513061*	*240*	*0.4*			*184*	*4.4*	*9.2*	*7.2*	*2.19*	*1.2*
482-8-11		Ata				18.726	15.555	38.339	*0.703370*	*0.513044*	*243*	*0.3*			*110*	*2.56*	*6.23*	*5.18*	*1.41*	*1.2*
482-8-12		Ata				18.729	15.565	38.356	*0.703440*	*0.513087*	*214*	*0.23*			*102*	*2.17*	*5.28*	*4.6*	*1.24*	*1.1*
26907		Tofua				18.608	15.557	38.210	*0.703400*	*0.513025*	*240*	*0.08*			*101*	*1.44*	*3.6*	*3.48*	*1.26*	*2.2*
26833		Tofua				18.454	15.536	38.088	*0.703460*	*0.513036*	*240*	*0.09*			*120*	*1.56*	*4.03*	*3.97*	*1.36*	*3*
26837		Tofua				18.542	15.549	38.165	*0.703480*	*0.513047*	*226*	*0.12*			*118*	*1.5*	*3.91*	*3.7*	*1.35*	*2.3*
FON31		Fonualei				18.593	15.549	38.224	*0.703810*	*0.512940*	*305*	*1.39*			*186*	*3.3*	*7.64*	*6.29*	*2.09*	*2.6*
FON39		Fonualei				18.576	15.549	38.202	*0.703760*	*0.512992*	*300*	*0.78*			*206*	*3.68*	*8.73*	*7.58*	*2.19*	*4.7*
FON11		Fonualei				18.593	15.549	38.224												
Late 7		Late				18.558	15.548	38.166	*0.703610*	*0.512954*	*235*	*0.31*			*99*	*1.4*	*3.64*	*3.11*	*1.07*	*2.2*
Late 13		Late				18.566	15.562	38.196	*0.703690*	*0.512942*	*225*	*0.63*			*165*	*2.9*	*7.1*	*5.45*	*1.9*	*2.3*
Late 2		Late				18.575	15.547	38.178												

[a] Italic values are from *Turner et al.* [1997].

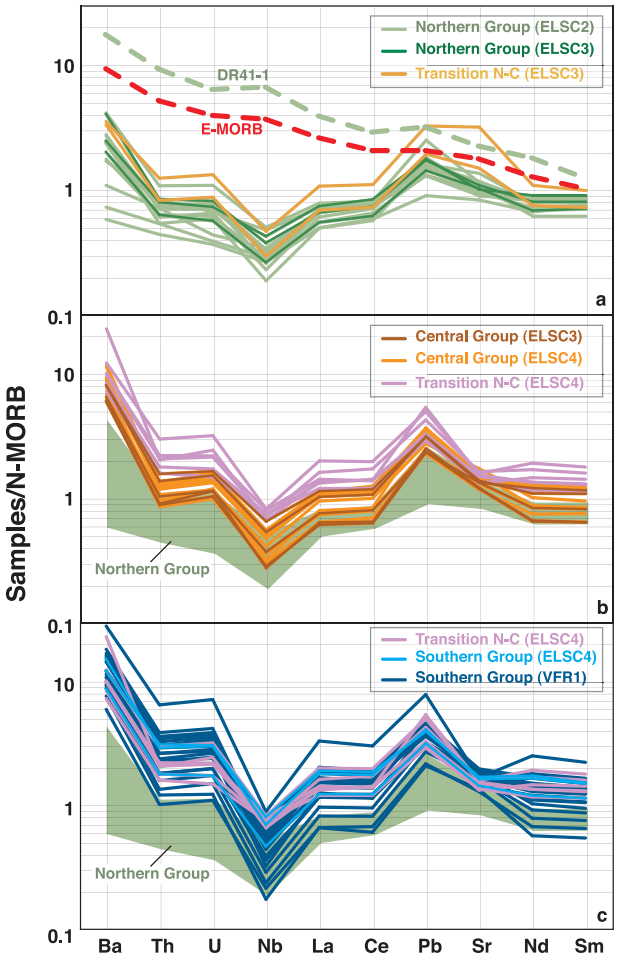

Figure 3. Trace element patterns normalized to N-MORB [*Sun and McDonough*, 1989]. Overall, the mobile trace element contents (e.g., Ba and Pb) increase from north to south. All samples but DR41-1 have a Nb depletion and a Ba and Pb enrichment consistent with a fluid-dominated subduction input. Four samples from the northern group (RC028, RC031, RC099, and RC107) have a pattern with a peculiar shape for the most incompatible elements, characterized by lower Ba/Th and higher Th/U ratios which could reflect the moderate E-MORB enrichment of a depleted mantle source. DR41-1, represented by the green dashed line, displays a pattern reflecting an enrichment in all the incompatible elements, very similar to the E-MORB pattern (red dashed line) from *Sun and McDonough* [1989].

ELSC3 to Valu Fa, the ridge is characterized by a well-defined axial high, with depth decreasing southward from 2200 m to 1800 m. The transition in ridge morphology correlates with the appearance of an axial magma chamber reflector in the southern part of the ELSC [*Harding et al.*, 2000; *Jacobs et al.*, 2007].

[10] Several Tonga islands are located within the latitudinal range of the Eastern Lau Spreading Center (Figure 1). Ata (south Tonga) is located about 50 km east of Valu Fa. Hunga Ha'apai and Hunga Tonga (two islands from the central Tonga, remnants of a submerged caldera) are located at the same latitude as the segment ELSC3 (~20.5°S) and ~80 km to the east. Kao and Tofua, two adjacent islands further to the north are located at the latitude of the segment ELSC1 (~19.7°S) and ~95 km to the east. Many submerged volcanoes have been observed along the arc front between the arc islands [*Stoffers et al.*, 2006].

3. Results

[11] We report 64 Pb-Sr-Nd isotopic ratios, trace element contents (i.e., Nb, Ba, La, Ce, Sm, Nd, Pb, Th and U) and Mg # obtained on glass chips from along-axis ELSC samples from 20.2 to 22.3°S (ELSC2 to VFR1) (Table 1), with an average spacing of ~3.6 km. We also report 13 new Pb isotopic compositions of Tonga arc samples previously analyzed by *Turner et al.* [1997]. Details on the analytical methods can be found in Appendix A.

[12] The trace element abundances, with the exception of sample DR41-1 (e.g., Figure 2), are within the range of the published back-arc data from the Lau basin, as are the Mg # (ranging from 0.67 to 0.16; with Mg # = Mg/(Mg+Fe)). Figure 2 shows that, except for DR41-1, the ELSC lavas display relatively lower enrichment in melt mobile elements (e.g., low La/Sm) than other BABB such as East Scotia and the Mariana Trough, despite stronger enrichment in fluid mobile elements (e.g., high Ba/Nb).

[13] The trace element patterns (Figure 3, see section 3.2 for the grouping definition) show an overall increase of the trace element contents toward the south, associated with enrichments in mobile elements (e.g., Ba and Pb) and relative depletions in HFSE (i.e., Nb) compared to the rare earth elements. These characteristics are all consistent with fluid-dominated subduction input increasing toward the south. Mobile/immobile element ratios normalized to N-MORB [*Sun and McDonough*, 1989] range from relatively depleted values ($(Ba/Nb)_N$~7 and $(U/Th)_N$~0.91, (Figure 3a)) in the northernmost segments to more enriched values ($(Ba/Nb)_N$~28 and $(U/Th)_N$~1.08) at Valu Fa (Figure 3c).

[14] A few samples present a trace element pattern not reflecting a fluid-dominated subduction input.

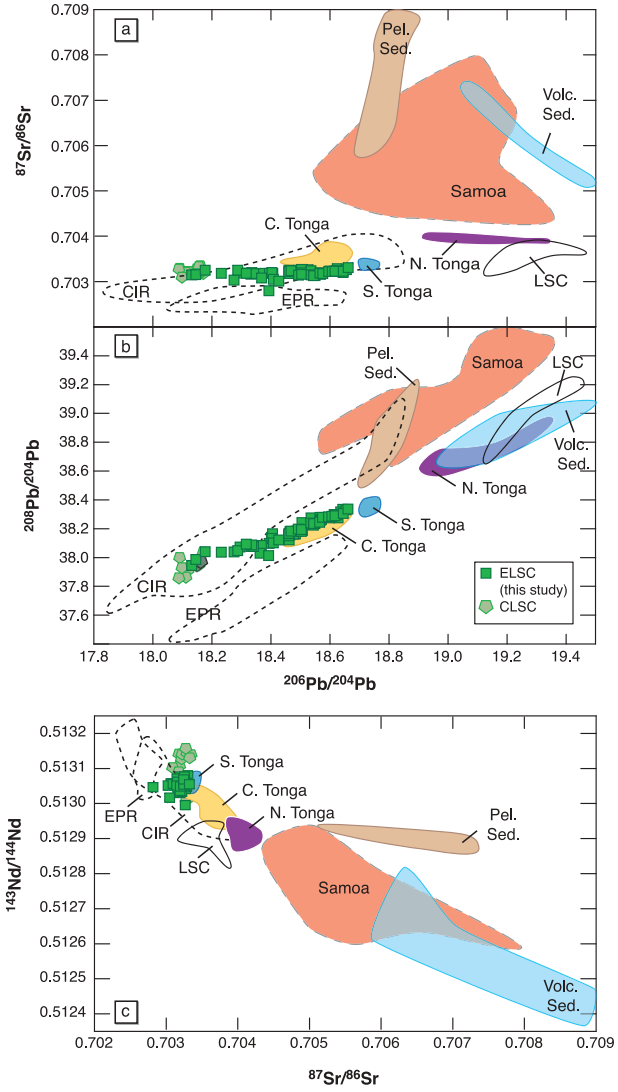

Figure 4. (a) $^{87}Sr/^{86}Sr$ and (b) $^{208}Pb/^{204}Pb$ versus $^{206}Pb/^{204}Pb$ and (c) $^{143}Nd/^{144}Nd$ versus $^{87}Sr/^{86}Sr$ diagrams illustrating the variability of our new ELSC isotope data relative to the East Pacific Rise and central Indian MORB, the Samoan lavas, the Tonga islands (south, Ata; central, Hunga Tofua, Kao, Late, and Fonualei; north, Tafahi and Niuatoputapu), the Louisville Seamount Chain (LSC), and the sediments from Site 204 (see Appendix C for data sources).

DR41-1 has a composition similar to the E-MORB of *Sun and McDonough* [1989] (Figure 3a), and plots on the E-MORB or OIB trend shown by the Samoa lavas (Figure 2). A few samples from segment ELSC2 have negligible subduction input and trace element patterns characterized by a smooth decrease from Ba to Nb followed by a smooth increase toward Pb (Figure 3a). These samples display the lowest trace element enrichment of ELSC2, along with particularly low $(U/Th)_N$ (<0.84) and $(Ba/Nb)_N$ (<3.6). Such trace element patterns are best explained by melting of a mantle source that has been depleted more than the source of the N-MORB reported by *Sun and McDonough* [1989], followed by some reenrichment in incompatible elements (hence the V-shaped patterns). These samples also display the lowest $^{206}Pb/^{204}Pb$ ratios measured in this study.

[15] In the following sections, we compare ratios of highly incompatible elements that are not significantly affected by melting or crystallization. The ELSC range of variation of these trace element ratios is much higher than what could be produced by different extents of melting of a single mantle source or by crystallization. As an example, 5% to 20% melting of the depleted DMM from *Workman and Hart* [2005] would generate a range in La/Sm of 0.71 to 0.95 and in Ba/La of 1.73 to 1.85 (Kd_{La} = 0.005, Kd_{Sm} = 0.033, Kd_{Ba} = 0.00024), while the ELSC samples range from 0.65 to 1.41 for La/Sm (excluding DR41-1) and from 2.9 to 43.3 for Ba/La.

[16] Pb isotope ratios range from 18.13 to 18.66 for $^{206}Pb/^{204}Pb$, from 15.50 to 15.56 for $^{207}Pb/^{204}Pb$, and from 37.95 to 38.35 for $^{208}Pb/^{204}Pb$. $^{87}Sr/^{86}Sr$ ratios vary from 0.70278 to 0.70332 with an average value of 0.70320 ± 0.00018 (2σ). By comparison, $^{143}Nd/^{144}Nd$ ratios show very little variation, ranging from 0.512983 to 0.513081 with an average value of 0.513056 ± 0.000030 (2σ), which represents a variability of less than 3 times the external reproducibility obtained on multiple analyses (n = 11) of DR41-1 (Table 1). Our new Pb-Sr-Nd isotopic analyses of Valu Fa samples have a compositional range similar to the on-axis samples reported by earlier studies [*Volpe et al.*, 1988; *Loock*, 1992; *Peate et al.*, 2001], except for $^{207}Pb/^{204}Pb$ ratios, which in our data set are lower on average and less variable.

[17] Our new Pb isotopic compositions measured in lavas from the central and south Tonga arc islands (from north to south: Fonualei, Late, Kao, Tofua and Ata) are consistent with the other more recent Pb analyses [*Hergt and Woodhead*, 2007; *Pearce et al.*, 2007] and with the analysis of one sample from Ata reported by *Jenner et al.* [1987] (see Figures B1–B3). As discussed in Appendix B, there are systematic discrepancies between the recent Pb isotopic ratios [*Pearce et al.*, 2007; this study] and the Pb isotopic ratios measured on the same samples earlier by [*Regelous et al.*, 1997; *Turner et al.*, 1997; *Ewart et al.*, 1998]. The results we report in this study significantly improve the Pb

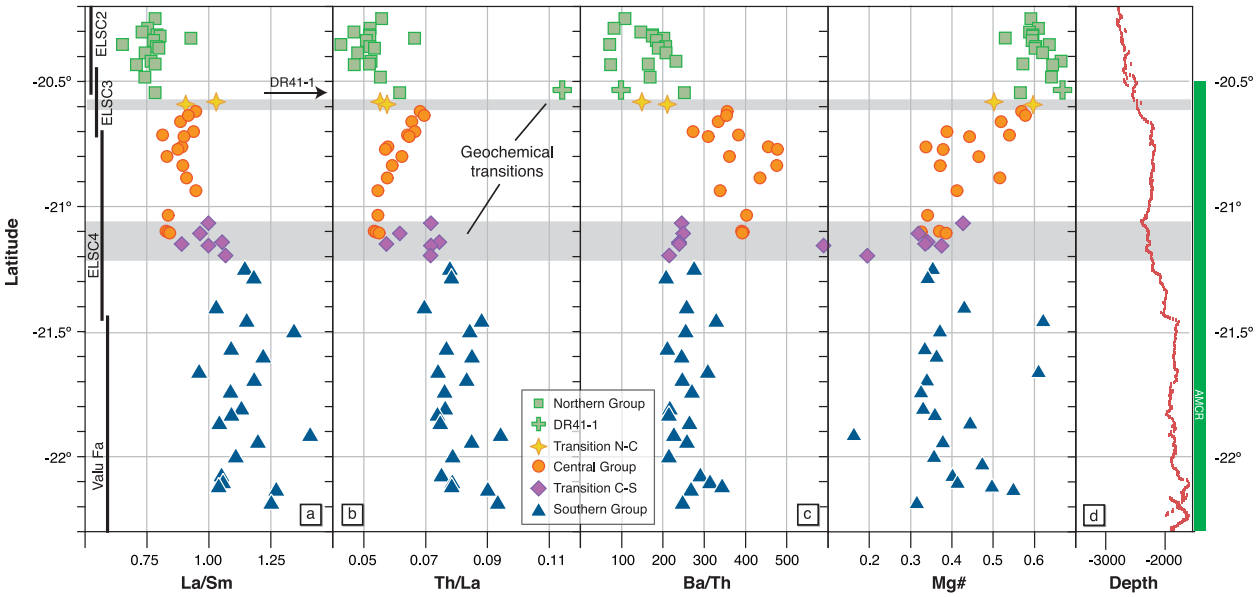

Figure 5. Along-axis variation of representative trace element ratios and Mg #, of depth [*Martinez and Taylor*, 2002] and the presence of an axial magma chamber reflector [*Harding et al.*, 2000; *Jacobs et al.*, 2007]. La/Sm reflects the enrichment in incompatible elements, Th/La reflects the sedimentary contribution to the arc magmas [*Plank*, 2005], and Ba/Th reflects the enrichment in mobile elements and the relative importance of fluid versus sediment melts. The samples are grouped as described in the text, on the basis of their geographic location and the existence of two important geochemical transitions. One transition is located within the ELSC3 and characterized by a jump in Ba/Th, Th/La, and La/Sm. The second transition is located in the middle of the ELSC4 and is characterized by a decrease in Ba/Th and an increase in Th/La, La/Sm, and $^{206}Pb/^{204}Pb$ ratio but not Ba/Nb. The apparent decoupling between Ba/Th and the other two ratios reflects a compositional change of the subduction input. Overall, the Th/La and La/Sm ratios increase from north to south showing a stronger subduction input closer to the arc front, and the Ba/Th ratio indicates a maximum fluid contribution in the central group.

isotopic data available from Tofua and Ata and allow comparison of the Lau back-arc and Tonga arc samples. The recent Pb isotopic data are shown in Figure 4 together with the existing Sr and Nd data.

[18] The new ELSC isotopic data are shown in Figure 4 together with Tonga island lavas, Samoan lavas, sediments from ODP Site 204, and the East Pacific Rise and central Indian MORBs. Despite significant Pb isotopic variability, the Sr and Nd isotope ratios in the ELSC lavas do not vary much compared to the MORB variability. Overall, the ELSC data define a trend from a low $^{206}Pb/^{204}Pb$ end-member plotting within the central Indian MORB field toward the Tonga arc fields (Figures 4a and 4b). In the Sr-Nd diagram (Figure 4c), the ELSC lavas plot within the central Indian Ridge field with slightly lower $^{143}Nd/^{144}Nd$ ratios than the CLSC lavas. The subducted sediments and the Samoan lavas display particularly radiogenic $^{87}Sr/^{86}Sr$ and unradiogenic $^{143}Nd/^{144}Nd$ ratios, more extreme than the ratios measured in the ELSC, CLSC or Tonga islands lavas.

3.1. Along-Axis Variation

[19] The trace element ratios show an increase in a subduction signature toward the south, as the distance to the arc decreases (Figure 5). To first order, the northern ELSC lavas have low enrichments of mobile trace elements, the central ELSC lavas have intermediate values and the southern ELSC (including Valu Fa) display much higher values (Figure 3). Within this overall framework of increasing arc component to the south, it is noteworthy that most of the geochemical variation related to the subduction input occurs within the segments ELSC3 and ELSC4, defining geochemical transition zones, and that different elements or ratios indicating a subduction signature do not increase in concert. The La/Sm ratio reflects the enrichment in incompatible elements not specifically related to fluid addition. It increases from 0.75 to >1.25 toward the south with significant jumps in the middle of ELSC3 and ELSC4 segments. The Th/La ratio also reflects enrichment in incompatible elements and can be used to identify a sedimentary contribution to the arc magmas

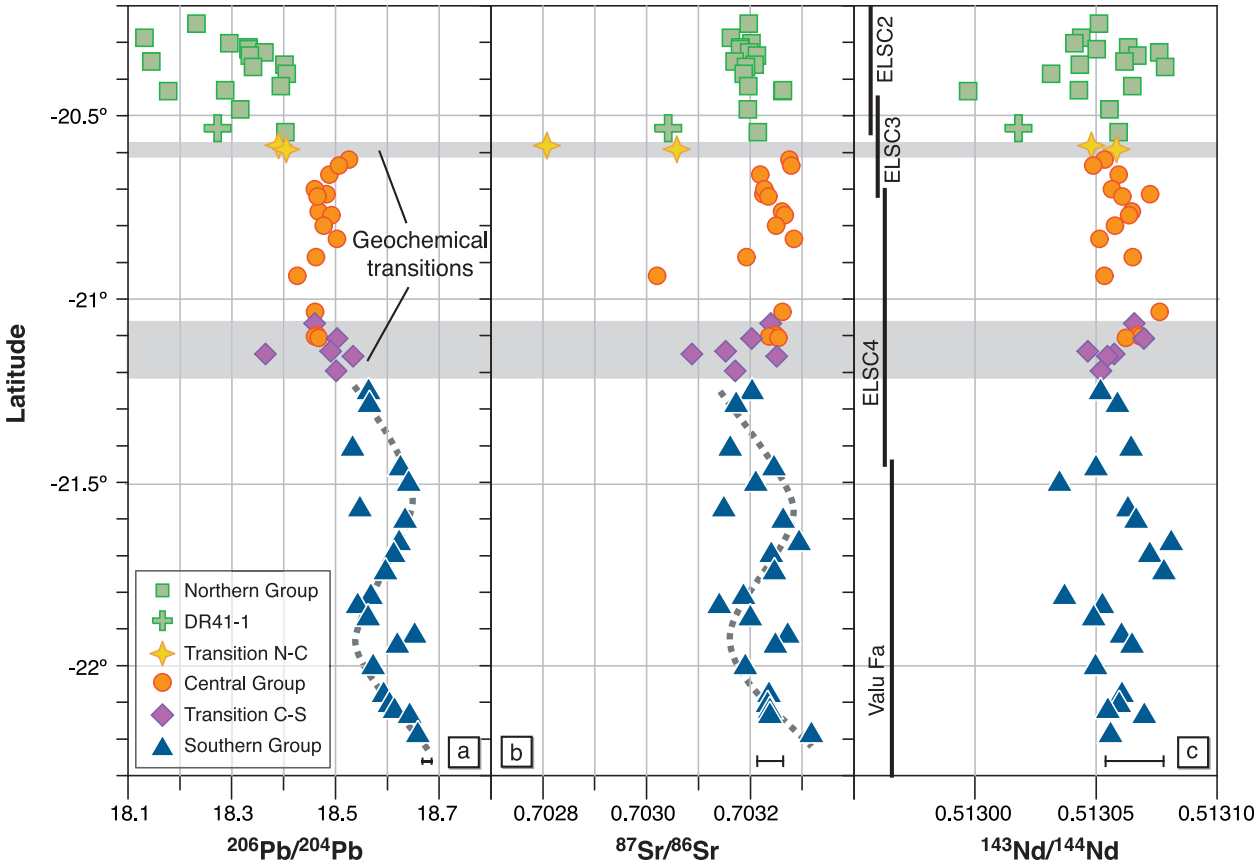

Figure 6. Along-axis variation of isotope ratios. The $^{206}Pb/^{204}Pb$ increases from north to south reflecting the increase of the subduction input. Except for a few samples, the $^{87}Sr/^{86}Sr$ ratios are relatively constant along the ELSC. $^{143}Nd/^{144}Nd$ is even less variable. The transition N-C is characterized by two samples with particularly low $^{87}Sr/^{86}Sr$. Within the central group, a spike in the $^{206}Pb/^{204}Pb$ ratios occurs just south of the transition N-C. The transition C-S, located in the middle of the ELSC4, is characterized by a southward increase in the $^{206}Pb/^{204}Pb$ ratios and slightly lower $^{87}Sr/^{86}Sr$. Within the southern group, most of the latitudinal variability of the $^{206}Pb/^{204}Pb$ and $^{87}Sr/^{86}Sr$ ratios can be described by a sinusoid, as indicated by the dashed lines.

[*Plank*, 2005]. It displays a similar latitudinal variation to La/Sm. On the other hand, the Ba/Th ratio characterizes the enrichment in fluid mobile elements and, combined with Th/La and La/Sm, shows that the fluid contribution to the subduction input increases in the middle of ELSC3 and seems to decrease in the middle of ELSC4. We show in succeeding diagrams and sections that these irregular variations are the result of variable amounts of subduction input of varying composition.

[20] The Pb isotope ratios increase toward the south with significant jumps in the middle of ELSC3 and ELSC4, from values similar to CLSC basalts (e.g., $^{206}Pb/^{204}Pb \sim 18.15$) to more radiogenic values consistent with existing Valu Fa data [*Volpe et al.*, 1988; *Loock*, 1992; *Peate et al.*, 2001] (Figure 6). At first glance, the $^{87}Sr/^{86}Sr$ and $^{143}Nd/^{144}Nd$ ratios do not show significant along-axis variation with latitude, which is not surprising since the samples from Valu Fa and CLSC display comparable Sr and Nd isotope ratios. However, some low $^{87}Sr/^{86}Sr$ "anomalies" are observed, often within or near the geochemical transition areas, and their origin is discussed below.

[21] On a smaller scale, the variations in trace element and isotope ratios show significant changes in subduction input over short distances where the distance to the arc does not change significantly. The southern group (see section 3.2 for the grouping definition) illustrates that the contribution of subduction input is only roughly related to the arc-ridge distance. The southern group lavas define correlations in the trace element and isotope diagrams (Figures 7–10) that reflect the mixture of the mantle wedge and the subduction input, but they show no systematic variation with the sample locations (e.g., higher mobile element enrichment closer to the arc front). In fact,

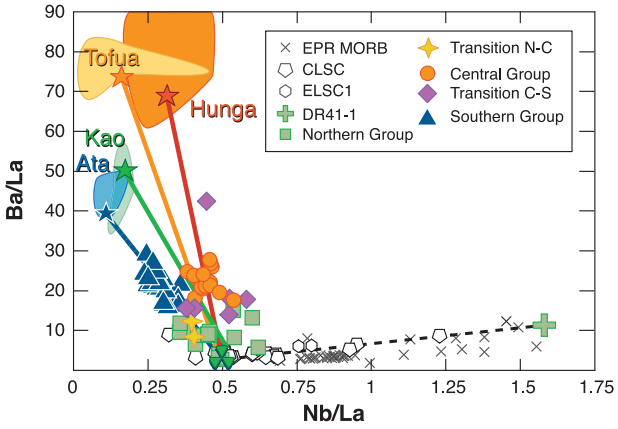

Figure 7. Ba/La versus Nb/La diagram (see Appendix C for data sources). The CLSC samples define a trend distinct from the samples from the ELSC segments (with the exception of DR41-1), pointing toward high Nb/La and moderate Ba/La. This trend is similar to that defined by the EPR MORB. The samples from the ELSC define trends pointing toward low Nb/La and high Ba/La, typical of arc lavas. In these plots, the arc islands located at the same latitude as the ELSC (i.e., Ata, Hunga, Kao, and Tofua) seem to extend the trends defined by the ELSC groups. In detail, the central group and the transition C-S define a trend distinct from the northern and southern groups, either pointing toward a more enriched mantle wedge composition (with higher Nb/La) or toward a subduction component with higher Nb/La (e.g., Hunga). Mixing lines between the different subduction end-members (stars, green for "S_{north}," orange for "$S_{central\text{-}N}$," red for "$S_{central\text{-}S}$," and blue for "S_{south}") and mantle wedge end-members (clovers, green for "M_{north}," orange for "$M_{central}$," and blue for "M_{south}") are also reported.

except for four samples, the latitudinal plots show that the along-axis variation of the isotope ratios reflecting the subduction component contribution (e.g., $^{206}Pb/^{204}Pb$) is best described by a sinusoid (Figure 6). The origin of the detailed latitudinal variation and its relationship with the mechanisms of the enrichment process, the ridge segmentation and morphology are addressed below in the discussion.

3.2. Enrichment Processes and Mantle Wedge Variability

[22] The trace element and isotope ratios (Figures 5 and 6) reveal that the ELSC south of 18.5°S can be divided into several geographical areas, within which the geochemical variations reflect mixtures between depleted mantle wedge and enriched components, often unique for each area. The area boundaries correspond to the two geochemical transitions located within segments ELSC3 and ELSC4. We thus define a northern Group, located between the ELSC3 transition and the northern extremity of the ELSC2, a central Group located between the two transitions, and a southern group located south of the ELSC4 transition. The samples within the transitions define two additional groups, namely, transition N-C (northern-central, i.e., the ELSC3 transition) and transition C-S (central-southern, i.e., the ELSC4 transition). Data from the CLSC and the northernmost segment of the ELSC (i.e., ELSC1) are also reported in Figures 7–12 as additional groups for comparison [*Falloon et al.*, 1992; *Volpe et al.*, 1988; *Peate et al.*, 2001; *Hergt and Woodhead*, 2007; *Pearce et al.*, 2007].

[23] The CLSC lavas display much less enrichment in fluid mobile elements compared to the ELSC segments (e.g., lower Ba/La, Figure 7). In fact, most of the CLSC lavas define a trend similar to East Pacific Rise MORB (Figures 7 and 8) pointing toward E-MORB-like compositions, which are characterized by enrichments in incompatible elements (i.e., melt mobile elements). *Peate et al.* [2001] have attributed the CLSC trace element and isotopic variations to a "water-rich component" different from the subduction-related component found in the southern ELSC, but still related in some way to active subduction processes. Only one sample (DR41-1) from our new sample set plots on this E-MORB trend, displaying a much higher degree of trace element enrichment than the CLSC. The other ELSC samples define a trend opposite in direction to the E-MORB trend in Figure 7, extending from the least enriched CLSC samples (low Nb/La and Ba/La) toward the Tonga arc island fields (high Ba/La, and lower Nb/La reflecting the apparent arc Nb depletion). This trend is consistent with a subduction-related enrichment in fluid mobile elements (i.e., Ba and to a lesser extent La, when compared to Nb).

[24] In detail, the geographical groups have specific trace element and isotopic features reflecting variations in the mantle wedge and subduction input. The northern group has the lowest trace element enrichment of the southern Lau basin, expressed by low incompatible element contents (Figure 3) and relatively depleted trace element ratios (Figure 5). The trace element and isotopic ratios show that the northern group defines a trend pointing from a depleted MORB-like composition toward an arc-like composition consistent with Kao (Figures 7–10). The mantle wedge (i.e., the low $^{206}Pb/^{204}Pb$ extremity of the trend) has an Indian-like composition characterized by high $^{208}Pb/^{204}Pb$, $^{207}Pb/^{204}Pb$

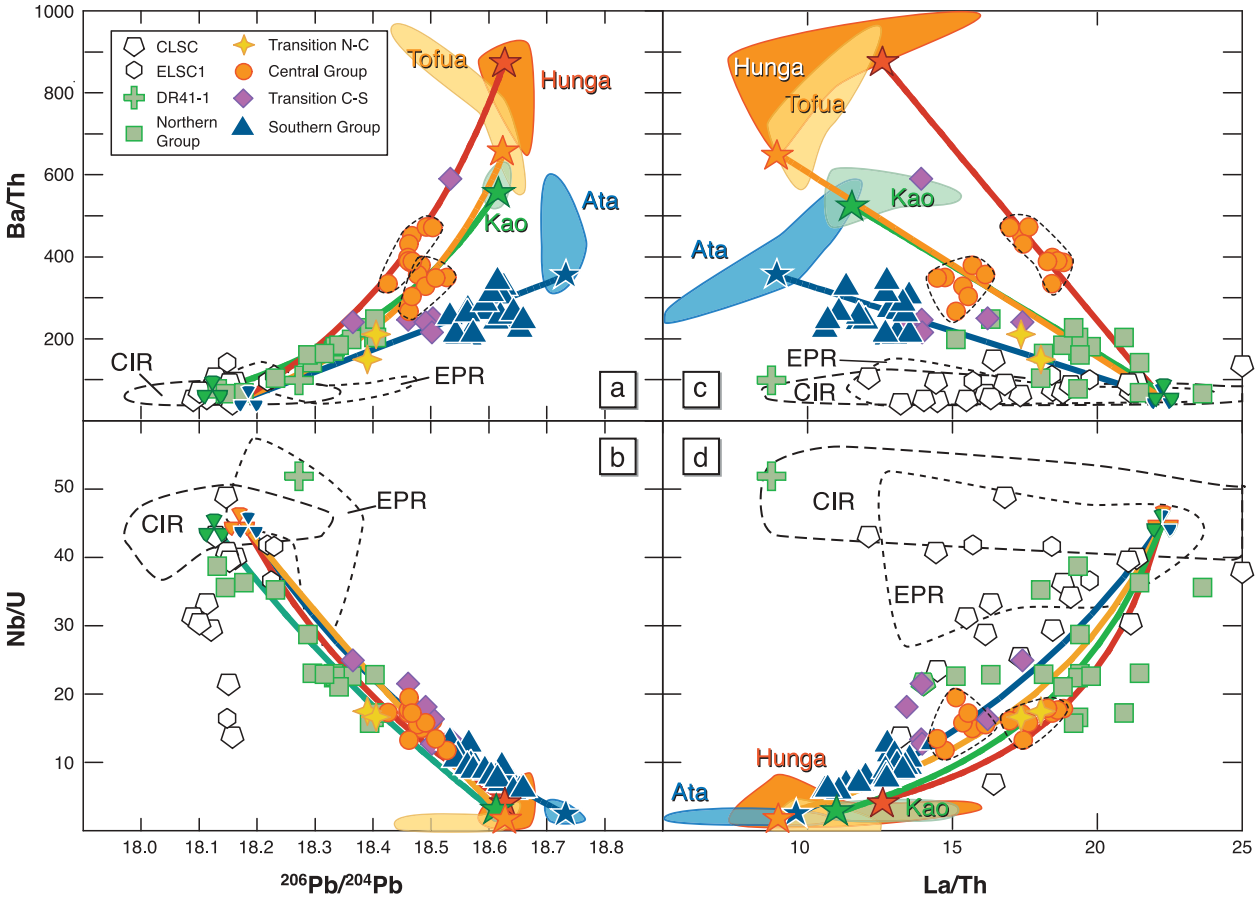

Figure 8. Ba/Th and Nb/U versus (a and b) $^{206}Pb/^{204}Pb$ and (c and d) La/Th (see Appendix C for data sources). The fields for the EPR and CIR (except the enriched samples located between 18°S and 20°S) are reported for comparison. The southern group points toward Ata, while the central and northern groups point toward subduction end-members, respectively, consistent with Hunga, Tofua, and Kao (symbols as in Figure 7).

and $^{87}Sr/^{86}Sr$ and low Ce/Pb for a given $^{206}Pb/^{204}Pb$ (Figures 9 and 10).

[25] The central group has a more pronounced subduction signature, with higher trace element contents, higher mobile element enrichment (Figure 3b) and higher $^{206}Pb/^{204}Pb$ (Figure 6). The central group samples have higher $^{206}Pb/^{204}Pb$, $^{207}Pb/^{204}Pb$, $^{208}Pb/^{204}Pb$ and $^{87}Sr/^{86}Sr$ ratios compared to the northern group (Figures 3, 8, and 9). In contrast, the Nd isotope ratios do not show any significant difference. In Figure 7, the central group is offset from the northern group toward higher Ba/La for a given Nb/La which could be explained either by a subduction-related end-member with higher Nb/La (similar to Tofua or Hunga) or by a mantle end-member slightly affected by an E-MORB-like enrichment similar to the one characterized by DR41-1 and the CLSC. In the Pb-Sr isotope diagrams (Figure 9c), the central group array requires that the central mantle wedge has a $^{87}Sr/^{86}Sr$ ratio lower than the northern mantle wedge and a subduction-related end-member within Tofua or Hunga fields. In detail, the trace element ratios involving Th reveal the existence of two subgroups within the central group. As illustrated in Figure 8, half of the samples from the central group (from the southern part of the area, i.e., the northern ELSC4, see Figure 5) display higher Ba/Th and La/Th with Nb/U and $^{206}Pb/^{204}Pb$ comparable to the other samples. While these samples have a similar range of Th contents, they contain slightly higher contents of the other incompatible elements.

[26] The transition N-C group includes two samples located in the middle of the segment ELSC3, with transitional trace element contents such as northern-like Ba/La and Th/La ratios and central-like La/Sm ratios. They have relatively high Sr content and low Sr isotope ratios that contrast with the surrounding sample groups, with the exception

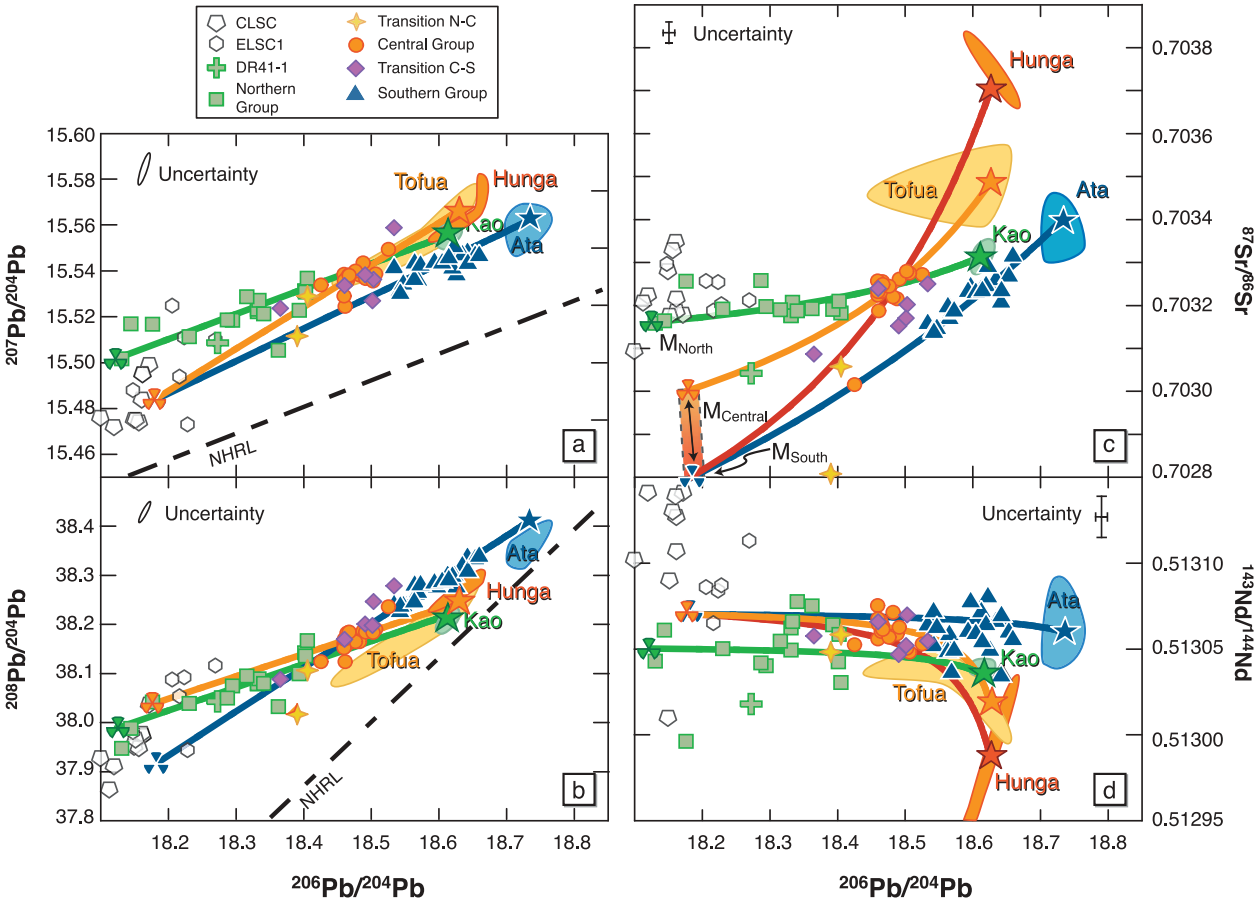

Figure 9. Diagrams of (a) $^{207}Pb/^{204}Pb$, (b) $^{208}Pb/^{204}Pb$, (c) $^{87}Sr/^{86}Sr$, and (d) $^{143}Nd/^{144}Nd$ versus $^{206}Pb/^{204}Pb$ with the ELSC, CLSC, and Tonga arc data (see Appendix C for data sources). The southern group defines good correlations in the Pb-Pb and Pb-Sr diagrams, pointing toward a subduction end-member similar to Ata. Linear interpolations through the southern group in the Pb-Pb diagrams point toward a mantle (blue clover) with a less Indian signature than the CLSC. It is, however, not Pacific-like as has been proposed by *Peate et al.* [2001] and *Pearce et al.* [2007]. The northern group points toward a mantle slightly more Indian-like (higher $^{208}Pb/^{204}Pb$ and $^{207}Pb/^{204}Pb$ for a given $^{206}Pb/^{204}Pb$) (green clover). Because of the absence of significant variation in $^{206}Pb/^{204}Pb$, the central group mantle end-member composition is not as well constrained but may be intermediate between the southern and northern mantle end-members. The ELSC and Tonga arc data do not present significant variation in $^{143}Nd/^{144}Nd$ which does not allow constraint of the mantle end-members' $^{143}Nd/^{144}Nd$ ratios. In the Pb isotopic plots, the dashed line represents the Northern Hemisphere Reference Line (NHRL) [*Hart*, 1984].

of DR41-1, which also has low $^{87}Sr/^{86}Sr$ and is located almost at the same latitude within ELSC2.

[27] The southern group includes the samples located south of the transition C-S. The samples have the highest trace element contents (Figure 3c) and the strongest subduction signature of the ELSC (e.g., the highest $^{206}Pb/^{204}Pb$ and Ba/La). While having the highest $^{206}Pb/^{204}Pb$, the southern group has particularly low Ba/Th and La/Th compared to other high $^{206}Pb/^{204}Pb$ ELSC lavas (Figure 8). Ata's lavas display a similar characteristic when compared to the central Tonga arc lavas. The chemical similarity between the southern group lavas and Ata is confirmed in the isotope diagrams where the southern group defines correlations pointing toward the composition of Ata (Figure 9). Extrapolation of trends shows that the mantle wedge in the southernmost part of the Lau basin has less of an Indian signature than the northern mantle wedge, and is characterized by lower $^{207}Pb/^{204}Pb$, $^{208}Pb/^{204}Pb$ and $^{87}Sr/^{86}Sr$ for a given $^{206}Pb/^{204}Pb$. In the trace element diagrams (Figures 7 and 8), the southern group points toward the northern group. Because of the strong enrichment in incompatible elements, it is difficult to constrain precisely the trace element composition of the southern mantle wedge. There are, however, some clues that the weaker Indian isotopic signature of the southern

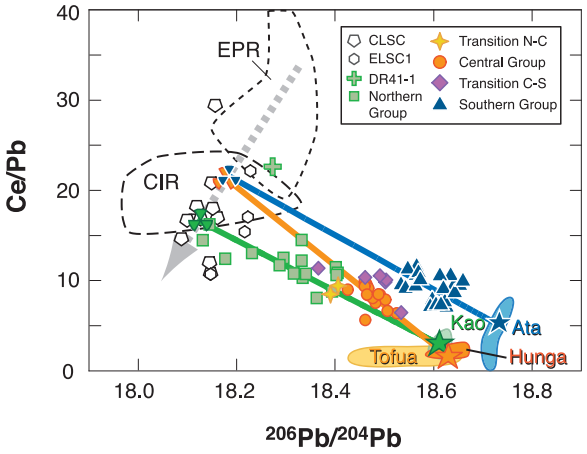

Figure 10. Ce/Pb versus $^{206}Pb/^{204}Pb$ diagram (see Appendix C for data sources). The ELSC and CLSC data are reported with the fields for the East Pacific Rise, central Indian Ridge (CIR, except the enriched samples located between 18°S and 20°S), and the Tonga arc islands Hunga. Tofua, Kao, and Ata. The dashed arrow represents the hypothetical change in Ce/Pb and $^{206}Pb/^{204}Pb$ ratios associated with a south to north increase in Indian-like signature (from EPR-like to CIR-like) that would explain the CLSC data. Using the constraints provided by the knowledge of the subduction end-member compositions, regressions through different groups (southern group is indicated by blue line, central group is indicated by orange line, and northern group is indicated by green line) and the intersections with the gray line can be used to estimate the Ce/Pb and $^{206}Pb/^{204}Pb$ ratios of the mantle wedge end-members, assuming that they plot along the dashed arrow.

mantle wedge is associated with a trace element composition slightly different from the northern mantle wedge (e.g., higher Ce/Pb, Figure 10).

[28] The transition C-S group includes the samples located within the transitional area of ELSC4 (Figures 5 and 6). They have trace element patterns intermediate between the two surrounding groups and plot either on the southern or central trends depending on the diagrams, reflecting the compositional change of subduction input (Ata-like for the southern group and Tofua/Hunga for the central group) and the transitional nature of the area. Isotopically, the transition C-S group defines a trend distinct from the other group trends in the $^{87}Sr/^{86}Sr$ versus $^{206}Pb/^{204}Pb$ diagram (Figure 9c). The trend is intermediate between the southern and central trend and points toward an intermediate low $^{87}Sr/^{86}Sr$ mantle wedge.

[29] To summarize, the ELSC trace element and isotopic variations reflect mixtures between a diversity of arc components and a mantle wedge that changes systematically from north to south. The mantle wedge variability is essentially characterized by a change in its isotope compositions which become more Indian-like toward the north. The along-axis variation in the subduction input tracks the latitudinal change of the Tonga arc island compositions (Ata, Hunga, Tofua and Kao).

4. Discussion

[30] These results demonstrate that the geochemical variability in the ELSC lavas is not due to a single subduction component whose amount varies with the distance form the arc. Instead, there are multiple trends corresponding to well-defined geographical areas, which require distinct mantle wedge and subduction-related end-members.

4.1. Compositions of the Subduction and Mantle Wedge End-Members Beneath the Eastern Lau Spreading Center

[31] The correlations for the different geographical groups in trace element and isotope diagrams, combined with the Tonga arc data set, can be used to constrain the compositions of four distinct subduction end-members ("S_{north}," "$S_{central\text{-}N}$," "$S_{central\text{-}S}$" and "S_{south}," defined by green, orange, red and blue stars, respectively, in Figures 7–11) and three distinct mantle wedge end-members ("M_{north}," "$M_{central}$" and "M_{south}," defined by green, orange, and blue clovers in Figures 7–10). Values are given in Table 2.

[32] We estimate the subduction-related end-member "S_{north}" to have a composition similar to Kao. The central group has two subduction-related end-members which differ by their enrichment in fluid mobile elements. This accounts for the apparent offset of central group data into two groups in Figures 8a, 8b, and 8d. "$S_{central\text{-}N}$," the subduction-related end-member for the northern part of the central group (southern ELSC3), has a trace element composition within Tofua's compositional range. For the southern part of the central group (northern ELSC4), "$S_{central\text{-}S}$" has a trace element composition within Hunga's range. "$S_{central\text{-}S}$" and "$S_{central\text{-}N}$" have similar Pb isotope ratios and "$S_{central\text{-}S}$" may have a more radiogenic $^{87}Sr/^{86}Sr$, mirroring the difference between Tofua and Hunga (shown in Figure 9 but not in Figure 11).

[33] The subduction-related end-member for the southern group "S_{south}" is relatively similar to Ata's trace element and isotope average [*Jenner et al.*, 1987; *Turner and Hawkesworth*, 1998;

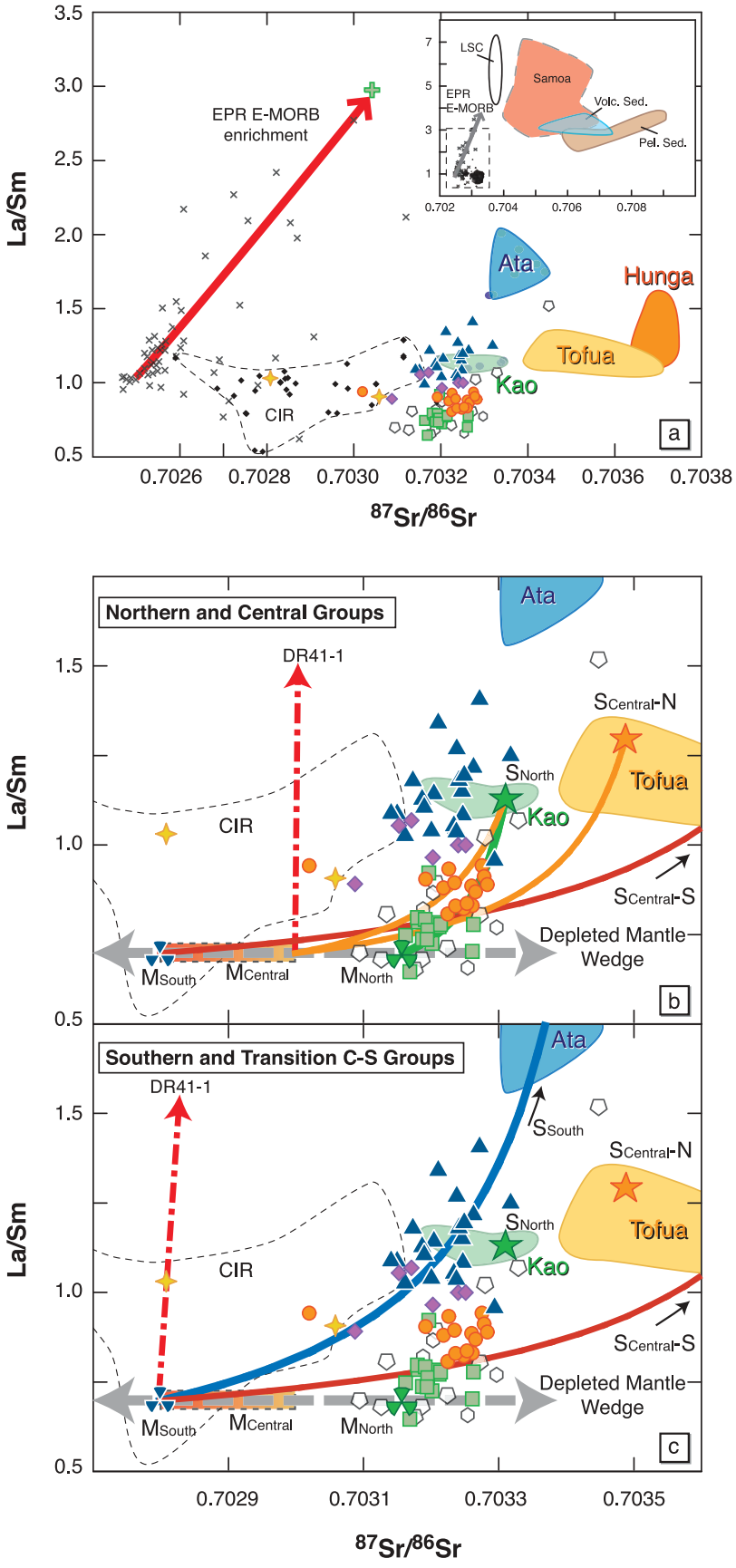
La/Sm
87Sr/86Sr
EPR E-MORB enrichment
CIR
Ata
Hunga
Tofua
Kao
LSC
Samoa
Volc. Sed.
Pel. Sed.
EPR E-MORB
a
Northern and Central Groups
DR41-1
SCentral-N
SNorth
SCentral-S
Depleted Mantle Wedge
MSouth
MCentral
MNorth
b
Southern and Transition C-S Groups
SSouth
c

Figure 11

Pearce et al., 2007], with a slightly higher $^{208}Pb/^{204}Pb$ (shown in Figure 9). Therefore the subduction component observed in the back arc changes systematically along with the variations of the volcanic front of the arc. More complete analyses of volcanic front volcanoes, including the submerged volcanic edifices can test and refine of these observations.

[34] "M_{north}" is defined in trace element composition by the most depleted samples showing a minimal subduction-related input. The central or southern groups do not include truly depleted samples so we must use projections to estimate "$M_{central}$" and "M_{south}" compositions. The southern group trends toward a mantle wedge end-member similar to the northern mantle wedge, except for slightly higher Ce/Pb (Figure 10). The trace element composition for "$M_{central}$" seems undistinguishable from "M_{south}." Overall, the difference in trace element compositions of mantle wedge end-members is small compared to the ELSC compositional range.

[35] The trends defined by the northern, central and southern groups in the Pb isotopes (Figure 9) and Ce/Pb versus $^{206}Pb/^{204}Pb$ diagram (Figure 10) can be used to determine the $^{206}Pb/^{204}Pb$ ratios of the mantle wedge end-members using the intersection of these trends with a hypothetical "MORB" trend. The "MORB" trend represents the transition between a Pacific-like mantle, and a central Indian-like mantle and is drawn to go through the low $^{206}Pb/^{204}Pb$ CLSC and ELSC samples. Determining the $^{206}Pb/^{204}Pb$ ratios in this way, the $^{207}Pb/^{204}Pb$ and $^{208}Pb/^{204}Pb$ ratios of the mantle wedge end-members can be constrained from the linear regressions in the Pb isotopic diagrams (Figures 9a and 9b). The northern mantle wedge lies at the most Indian-like extremity of the CLSC-ELSC1 field and the southern mantle wedge "M_{south}" has a composition that is less Indian-like and still within the CLSC range. While using a lower Ce/Pb for the southern subduction end-member in Figure 10 would apparently put the southern mantle wedge within the EPR field, the well defined $^{208}Pb/^{204}Pb$-$^{206}Pb/^{204}Pb$ correlation lying well above NHRL shows that it cannot be Pacific-like in Pb isotope composition (Figures 9a and 9b). The regressions though the central group in the Pb isotope diagrams, while not tightly constrained, show that "$M_{central}$" is likely intermediate between "M_{south}" and "M_{north}."

[36] The Sr isotope ratio of the mantle wedge end-members is the only unconstrained parameter and we can determine for the different groups which value provides the best fit in Figure 9c. "M_{north}" appears to have a $^{87}Sr/^{86}Sr$ within the range of the northern ELSC and CLSC samples and "M_{south}" a $^{87}Sr/^{86}Sr$ significantly lower than the CLSC range ($^{87}Sr/^{86}Sr \sim 0.7028$). The $^{87}Sr/^{86}Sr$ ratio of the central mantle wedge is dependent on our choice of the $^{87}Sr/^{86}Sr$ for the subduction end-member. With $^{87}Sr/^{86}Sr$ varying between "$S_{central\text{-}S}$" and "$S_{central\text{-}N}$," the $^{87}Sr/^{86}Sr$ calculated for "$M_{central}$" remains intermediate between "M_{south}" and "M_{north}," with $^{87}Sr/^{86}Sr$ of ~0.7028 and 0.7030, respectively (Figure 9c).

[37] The absence of a significant variation in $^{143}Nd/^{144}Nd$ does not permit us to use a method equivalent to the one used for Sr isotopes. *Pearce et al.* [2007] have shown convincingly that the subduction components contribute significantly to the Nd budget of the arc and back-arc lavas found in the Lau basin, which is confirmed by our new trace element data. The higher mobility of Pb is

Figure 11. La/Sm versus $^{87}Sr/^{86}Sr$ illustrating the different processes responsible for the ELSC lava compositional variations (see Appendix C for data sources). (a) The range of variation of the Tonga arc islands, the EPR (small cross) and CIR basalts (dashed field and small diamonds, except the enriched samples located between 18°S and 20°S), the Samoan lavas, the Louisville Seamount lavas, and the volcaniclastic and pelagic sediments relative to ELSC and CLSC data. Symbols for the ELSC samples are as in Figures 7–10. DR41-1 plots on the E-MORB end of the EPR trend (red arrow in Figure 11a). (b and c) These plots zoom in on the ELSC and CLSC data and are used to illustrate the models discussed in the text. In these plots, the double gray arrow represents the change in Indian signature of the depleted mantle wedge with no change in La/Sm. The mixing hyperbola between the northern mantle wedge "M_{north}" and "S_{north}" (Figure 11b) goes through most of the northern group data. The mixing hyperbolae between the central mantle wedge "$M_{central}$" (represented by a rectangle with a color gradient like in Figure 9c) and the southern subduction components "$S_{central\text{-}N}$" and "$S_{central\text{-}S}$" plot below the central group data suggesting that "$M_{central}$" may be slightly offset toward higher La/Sm consistent with the contribution of a small amount of enriched component similar to DR41 (vertical red dashed arrow). In Figure 11c, the mixing hyperbola between "M_{south}" and "S_{south}" goes through the southern group data. The mixing hyperbolae between "M_{south}" with "S_{south}" and "$S_{central\text{-}S}$" encompass the transition C-S data reflecting the change in the subduction input composition. It shows that the mantle wedge of the transition C-S group likely has a $^{87}Sr/^{86}Sr$ ratio similar to the southern group.

Table 2. Pb, Sr, and Nd Ratios and Trace Element Contents of the End-Members Used for the Mixing Calculation[a]

	$^{206}Pb/^{204}Pb$	$^{207}Pb/^{204}Pb$	$^{208}Pb/^{204}Pb$	$^{87}Sr/^{86}Sr$	$^{143}Nd/^{144}Nd$	Sr (ppm)	La (ppm)	Ce (ppm)	Nd (ppm)	Sm (ppm)	Nb (ppm)	Ba (ppm)	Pb (ppm)	Th (ppm)	U (ppm)
Kao average	18.613	15.556	38.212	0.703314	0.513040	252	2.37	6.81	6.23	2.11	0.41	118	2.3	0.214	0.155
	± 0.006	± 0.002	± 0.01	± 0.000025	± 0.000015	± 28	± 0.35	± 0.45	± 0.79	± 0.12	± 0.02	± 3	± 0.5	± 0.016	± 0.018
Tofua average	18.563	15.554	38.184	0.703496	0.513031	228	1.60	4.18	3.92	1.40	0.15	122	2.5	0.152	0.135
	± 0.084	± 0.016	± 0.078	± 0.000096	± 0.000015	± 13	± 0.37	± 1.26	± 0.59	± 0.35	± 0.24	± 30	± 0.4	± 0.043	± 0.023
Hunga average	18.638	15.567	38.274	0.703685	0.512988	179	1.56	4.21	3.52	1.28	0.46	136	1.6	0.161	0.158
	± 0.080	± 0.026	± 0.075	± 0.000220	± 0.000112	± 12	± 0.59	± 1.80	± 1.09	± 0.34	± 0.29	± 55	± 0.4	± 0.072	± 0.023
Ata average	18.725	15.559	38.353	0.703374	0.513063	236	3.16	7.37	5.79	1.71	0.39	141	1.92	0.354	0.177
	± 0.015	± 0.005	± 0.023	± 0.000040	± 0.000018	± 54	± 0.94	± 1.81	± 1.98	± 0.44	± 0.18	± 41	± 1.45	± 0.062	± 0.036
S_{north}	18.613	15.556	38.212	0.703314	0.513040	252	2.54	6.81	6.23	2.11	0.41	118	2.3	0.214	0.155
$S_{central}$ (A)	18.627	15.565	38.242	0.703475	0.513031	228	1.60	4.18	3.92	1.40	0.15	122	2.5	0.152	0.135
$S_{central}$ (B)	18.627	15.565	38.242	0.703700	0.512988	190	1.9		4.43	1.56	0.6	130		0.15	0.135
S_{south}	18.735	15.562	38.410	0.703374	0.513063	236	3.05	6.5	5.4	1.50	0.325	120	1.3	0.34	0.15
M_{north}	18.126	15.502	37.988	0.70316	~0.51305	80	1.6	5.7	6.10	2.3	0.8	5	0.345	0.072	0.018
$M_{central}$	18.180	15.484	38.039	0.70300	~0.51307	82	1.7	5.9	6.40	2.31	1.0	6.5	0.275	0.087	0.022
M_{south}	18.186	15.484	37.918	0.70280	~0.51307	70	1.6	5.7	6.10	2.3	0.8	4	0.265	0.072	0.018

[a] Tonga Island averages are calculated using the recent Pb data [*Hergt and Woodhead*, 2007; this study] and the Sr, Nd isotope, and trace element data from *Turner et al.* [1997], *Ewart et al.* [1998], and *Hergt and Woodhead* [2007]. See text for details on the estimate of the Pb and Sr isotopic ratios.

responsible for a high Pb/Nd ratio in the subduction input, which would be expressed by a mixing hyperbola with strong curvature between the mantle and subduction end-members. Since the southern group and Ata plot within the same $^{143}Nd/^{144}Nd$ range (~0.51306 ± 0.0003, Figure 9d), it implies that "M_{south}" and "S_{south}" have similar Nd isotopic compositions. We chose $^{143}Nd/^{144}Nd$ ~0.51307 for "M_{south}." The central Tonga arc islands have slightly less radiogenic $^{143}Nd/^{144}Nd$ ratios compared to the northern and central groups. Because of the curvature of the mixing hyperbolae (not shown) in the $^{143}Nd/^{144}Nd$-$^{206}Pb/^{204}Pb$ diagram, "M_{north}" and "$M_{central}$" likely have a higher $^{143}Nd/^{144}Nd$ than "S_{north}" and "$S_{central}$," between 0.51304 and 0.51310. "$M_{central}$" seems indistinguishable from the southern mantle wedge "M_{south}" while the low $^{206}Pb/^{204}Pb$ samples suggest that "M_{north}" has a $^{143}Nd/^{144}Nd$~0.51305.

4.2. Origins of the Mantle Wedge Variability

[38] At the basin scale, the mantle wedge isotopic composition changes systematically, displaying an increasing Indian-like signature from south to north. DR41-1 and a few samples from the central, northern and transition C-S groups provide evidence for enrichments in incompatible elements similar to enriched mid-oceanic ridge basalts (having slightly higher Nb/La and Ba/La than the southern group and most of the northern group samples, Figure 7). DR41-1 has an isotopic composition within the ELSC range despite its extreme trace element contents so the trace element enrichment does not appear to significantly affect the isotope ratios. Therefore, these two processes that affect the mantle wedge (change from Indian to Pacific mantle and enrichment akin to E-MORB) do not seem to be simply related and their origin is discussed below.

4.2.1. Southward Flow of Indian Mantle Progressively Replenishing the Mantle Wedge

[39] The data from the various ODP Sites, which sampled the early volcanic products of the back arc [*Ewart et al.*, 1994b; *Hergt and Farley*, 1994; *Hergt and Hawkesworth*, 1994; *Ewart et al.*, 1998; *Pearce et al.*, 2007], and the along-axis samples [*Falloon et al.*, 1992; *Volpe et al.*, 1988; *Peate et al.*, 2001; *Hergt and Woodhead*, 2007; *Pearce et al.*, 2007] provide evidence for the presence of an initially Pacific-like mantle which

has been replaced by an Indian-like mantle migrating southward. For example, data from ODP Site 834, located on the older part of the oceanic crust formed by the Lau spreading centers (Figure 1) at the same latitude as the CLSC, define a linear trend in Pb-Pb isotope diagrams toward the Pacific MORB field (Figure 12). This result remains true even with the analytical bias between the ODP Pb isotope data and the recent Pb analyses and contrasts with the Indian-like signature measured in the lavas recently erupted along the CLSC.

[40] Our new isotope results confirm the existence of a latitudinal change of the mantle wedge isotopic composition along the ELSC. The interpolated mantle wedge compositions for the ELSC groups show that the strength of the Indian-like signature changes along the Eastern Lau Spreading Center, becoming stronger toward the north (for example, seen in $^{206}Pb/^{204}Pb$ versus $^{208}Pb/^{204}Pb$ in Figure 9). The interpolation of the southern group trend also reveals that the mantle wedge beneath the southern Lau basin displays an Indian-like signature and that Pacific-like signature similar to the ODP Site 834 is not observed anywhere along the Eastern Lau Spreading Center (Figure 12). Since we have not analyzed samples from the southernmost segment of Valu Fa (VFR2), we cannot preclude the possibility of finding such a signature at the southernmost extremity of the Lau basin. While there is some uncertainty on the Pb isotope ratios of the central mantle wedge, it has clearly $^{87}Sr/^{86}Sr$ intermediate between southern and northern. This result is consistent with a progressive southward increase of the Indian-like isotopic signature and suggests that the trace element enrichment of the mantle wedge does not have a major effect on the mantle wedge isotopic compositions.

[41] *Pearce et al.* [2007] have proposed on the basis of Nd and Hf isotopic variations that the mantle migrating southward in the Lau basin is heterogeneous, containing easily fusible "plums" of enriched material that are progressively extracted by melting during the southward migration. Our samples do not display significant $^{143}Nd/^{144}Nd$ variations which would be expected if the model proposed by *Pearce et al.* [2007] was valid at the ELSC scale. In Figure 11, the interpolated mantle wedge compositions plot along a horizontal trend (i.e., displaying little La/Sm variation with significant Sr isotope variation) showing that the isotopic variation of the mantle wedge along the ELSC reflects the southward flow of a depleted Indian-like mantle that is not carrying "plums" of enriched material.

4.2.2. Origin of the Trace Element E- MORB-Like Enrichment

[42] The process responsible for the enriched trace element signature of DR41-1 could be responsible for a milder enrichment affecting locally the mantle wedge beneath the central, northern and transition C-S groups. Adding ~1.5–3% of DR41-1 to southern or northern mantle wedge end-members gives a slightly enriched mantle composition that could explain the distinct trend defined by the central group and a few depleted samples from the main trend in Figure 7, with almost no effect on the isotopic compositions. Figure 11b also suggests a mild trace element enrichment of the central mantle wedge. The two mixing hyperbolae between the extreme compositions for "$M_{central}$" with "$S_{central\text{-}S}$" and "$S_{central\text{-}N}$" plot below the central group data. A slightly enriched mantle wedge end-member with a higher La/Sm (0.8 instead of 0.7) would move the hyperbola closer to the central group data. This enrichment is not evident elsewhere, since the mixing hyperbola between the other mantle and subduction-related end-members do provide a good fit of the corresponding data.

[43] Understanding the origin of DR41-1's extreme composition is therefore pertinent to the nature of the enrichment process affecting part of the mantle wedge. DR41-1 trace element pattern is very similar to E-MORB (Figure 3), suggesting a possible common origin. The origin of the E-MORB enrichment is still a matter of debate, either attributed to recycling of crustal materials [*Hofmann and White*, 1982; *Allègre*, 1987; *Weaver*, 1991] or to mantle metasomatism by low-degree melts [*Hawkesworth et al.*, 1984; *Hart*, 1988; *Donnelly et al.*, 2004]. DR41-1 has a lower $^{87}Sr/^{86}Sr$ than the surrounding samples (but still within the ELSC range) and "M_{north}" which implies that the component responsible for its enriched trace element composition has an even lower $^{87}Sr/^{86}Sr$ (Figure 9c). This precludes an ancient enrichment process of the mantle wedge, which would have developed more radiogenic $^{87}Sr/^{86}Sr$ with time. The enriched component has thus to be added recently to the mantle wedge. It also implies that the recycled pelagic and volcaniclastic sediments and the Louisville Seamounts, which have too radiogenic $^{87}Sr/^{86}Sr$ ratios, cannot be the source of the enriched component. Figure 10 shows that DR41-1 has a less

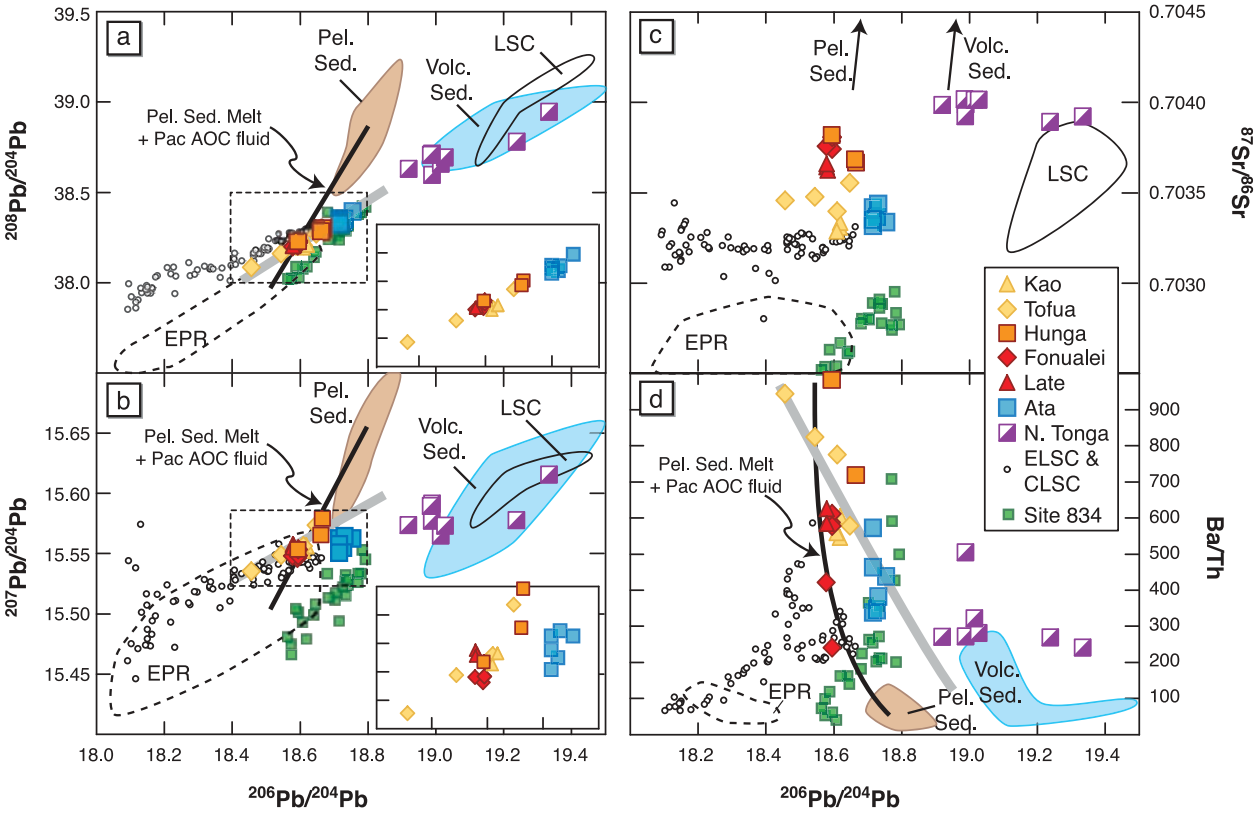

Figure 12. Diagrams explaining the origins of variations in components of the Tonga arc: (a) $^{208}Pb/^{204}Pb$, (b) $^{207}Pb/^{204}Pb$, (c) $^{87}Sr/^{86}Sr$, and (d) Ba/Th versus $^{206}Pb/^{204}Pb$ (see Appendix C for data sources). Only the samples with recent Pb data are reported for the Tonga arc islands. These diagrams illustrate the range of variation of the south, central and north Tonga islands relative to the ELSC and CLSC data and the ODP site 834. The fields for the pelagic and volcaniclastic sediments from the ODP Site 204, the Louisville Seamount Chain lavas (LSC, data from Georoc), and the East Pacific Rise MORB (data from PetDB) are also reported. As developed in Appendix B, there is a significant discrepancy between the recent Pb data and the data collected by *Ewart et al.* [1998], *Regelous et al.* [1997], and *Turner et al.* [1997]. Despite the fact that the sediment Pb data have only been reported by these authors, the offset between the old and recent Pb data is not large enough to displace significantly the pelagic and volcaniclastic sediment fields. The south Tonga island Ata displays higher $^{206}Pb/^{204}Pb$ than the central Tonga islands, consistent with a significant contribution of the volcaniclastic sediments associated with the subducted Louisville Seamounts Chain, currently located beneath the island (see Figure 1). Tofua's data define a trend (gray line) pointing toward a subduction end-member intermediate between the pelagic and volcaniclastic sediments. It is possible that a small amount of volcaniclastic sediment contributes to Tofua and Kao's lavas. Farther north, Fonualei and Late plot on the hypothetical mixing line (thick black line) between a fluid derived from the subducted Pacific Altered Oceanic crust and a pelagic sediment melt, suggesting the absence of volcaniclastic sediment contribution.

Indian-like (i.e., higher Ce/Pb) than the northern mantle wedge and higher $^{206}Pb/^{204}Pb$. It has however a Pb isotope composition within the range of the other ELSC, plotting between the northern and southern trends (Figure 9). This combination precludes the subducted Pacific oceanic crust as the origin of the enriched component. While it may have the appropriate Ce/Pb, the subducted altered Pacific oceanic crust has an inappropriate Pacific-like Pb isotopic signature (i.e., low $^{208}Pb/^{204}Pb$ and $^{207}Pb/^{204}Pb$ for a given $^{206}Pb/^{204}Pb$) and too radiogenic $^{87}Sr/^{86}Sr$ (~0.70475 [*Staudigel et al.*, 1996]). The enriched component must therefore be a low-degree melt derived from a mantle with an isotopic composition slightly less Indian-like than "M_{north}," similar to what is observed farther south in the Lau basin. The subducting slab is dragging down the mantle located just above it and imposes a west-to-east mantle flow [*Conder et al.*, 2002]. Combined with the progressively increasing Indian-like signature of the back-arc lavas mantle source, this implies than the mantle dragged to depth has a slightly less Indian-like signature than what is currently found at shallower depth (Figure 14).

[44] Low-degree melts derived from a deeper section of the mantle wedge and preconditioning of the central and transition C-S mantle wedge explains both the trace element enrichment and the absence of significant isotopic change. The west-to-east mantle streamlines (as reported by *Conder et al.* [2002, Figure 3]) requires that the preconditioning happened while the mantle flowing toward the melting regime beneath the spreading center was located farther west and slightly deeper.

[45] The origin of these low-degree melts could be related to the release of a small amount of fluid by the subducted slab that would induce melting of the deeper part of the mantle. The absence of significant enrichment in fluid mobile element in DR41-1 however requires that the fluid has negligible effect on the trace element budget which mainly reflects the low-degree melts of the mantle wedge. The melts produced would ascend vertically, not reaching the surface and preconditioning the upper part of the wedge before it arrives in the melting regime beneath the ridge.

4.3. Identification of the Subduction Components in the Lau Basin–Tonga Arc System

[46] The combination of our new ELSC trace element and isotopic data set with recent Tonga arc Pb isotopic data [*Hergt and Woodhead*, 2007; *Pearce et al.*, 2007] provides new constraints on the nature of the subduction components in the Lau Basin–Tonga arc system, and on the origin of the geochemical variability of the central and south Tonga arc lavas. The ELSC mixing trends (Figures 7–11) require several subduction end-members. The compositional variability of these end-members has to be produced by variable contributions of at least two subduction-related components. The same distinct components that affect the central and south Tonga arc influence the corresponding sections of the ELSC. These relationships also show that the subduction input to the mantle wedge is spatially organized in a way that varies along the arc and is continuous across the arc. It is of interest to consider the causes of the variations in the subduction components along the arc.

[47] The central Tonga arc data reveal that the lowest $^{206}Pb/^{204}Pb$ compositions in the arc (at Tofua) are associated with low Ce/Pb ratios (Figure 10) which can be explained if the Pb budget in the arc lavas is dominated by a mixture between a fluid (with low Ce/Pb and low $^{206}Pb/^{204}Pb$) derived from altered oceanic crust (AOC), and a sediment partial melt (Figure 12).

[48] In comparison to the central Tonga arc, the south Tonga arc data (Ata) have higher $^{206}Pb/^{204}Pb$ and $^{208}Pb/^{204}Pb$ with similar $^{207}Pb/^{204}Pb$. To explain this difference, there could be a contribution from the subducting Louisville Seamount Chain (LSC) or the associated volcaniclastic sediments (Figures 12b and 12c). The projected location of the LSC onto the subducted Pacific plate shows that it is currently beneath Ata (Figure 1). This localized effect of the LSC is not consistent with an LSC influence in the north Tonga arc [*Regelous et al.*, 1997; *Turner et al.*, 1997], which would require a 4 Ma delay in the influence of the subduction components. Such a long time is also inconsistent with the short transport times inferred from U-Th isotope disequilibria [*Turner et al.*, 1997]. Instead, the northern Tonga islands must be influenced by another subducted enriched material unrelated to the LSC, possibly the volcanic chain subducting between 18 and 18.5°S.

[49] The four Tofua samples with new reliable Pb isotope data define trends in the Ba/Th versus $^{206}Pb/^{204}Pb$ and Pb isotope diagrams that are inconsistent with simple mixing between an AOC fluid and a pelagic sediment melt (Figure 12). The high $^{206}Pb/^{204}Pb$ and low Ba/Th end-member, attributed to sediment melt [*Turner et al.*, 1997], needs an isotope composition intermediate between the pelagic and volcaniclastic sediments. It is possible that a small proportion of the sediments currently subducting at Tofua's latitude have a volcaniclastic origin. At the other extremity of the Tofua trend, the fluid related end-member with high Ba/Th and low $^{206}Pb/^{204}Pb$ does not plot within the Pacific MORB field (Figure 12). A simple explanation for this offset could be that the fluid contains contributions from both the altered oceanic crust and sediment. This has been proposed by *Hergt and Woodhead* [2007] on the basis of the relatively high $^{206}Pb/^{204}Pb$ ratio of the high Ba/Th end-member.

[50] Hunga, the island located between Tofua and Ata, displays similar Pb isotope variation to Tofua associated with higher $^{87}Sr/^{86}Sr$ and Ba/Th (Figure 12). The data suggest involvement of the same components with higher fluid contribution.

[51] Kao, the island located next to Tofua (Figure 1), displays no significant Pb isotope variation and plots within Tofua's field in most diagrams, suggesting a relatively similar geochem-

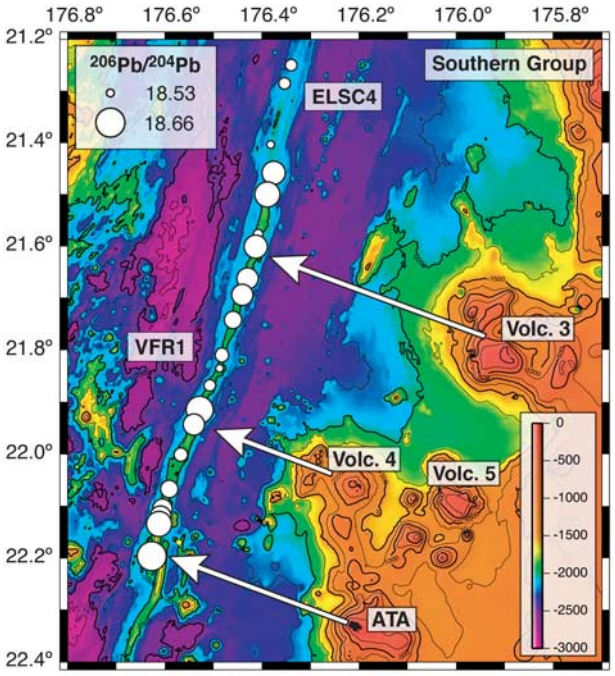

Figure 13. Map of the southern part of the ELSC (southern group) illustrating the change in $^{206}Pb/^{204}Pb$ along the axis. The highest $^{206}Pb/^{204}Pb$ ratios are located above the same downgoing slab flow lines as Ata, volcano 4, and volcano 3. It strongly suggests that the subduction input observed in the southern ELSC and the south Tonga arc volcanoes has a common origin.

ical history and the involvement of the same components. However, for a given Ba/Th (i.e., a given fluid contribution in the subduction input), Kao lavas have lower $^{87}Sr/^{86}Sr$, which suggests a smaller sedimentary contribution to the fluid (Figure 12c). Both islands have similar Nd isotope ratios, supporting the idea that their differences are related to the fluid-related subduction components and not to the mantle wedge.

[52] Farther north, two other islands from the central Tonga arc, Fonualei and Late, show isotope variations that extend the complexity of the processes responsible for the subduction input. Late and Fonualei lavas show almost no variation in Pb isotope ratios (Figure 12). They have slightly lower Ba/Th and higher $^{87}Sr/^{86}Sr$ compared to Kao and Tofua for a given $^{206}Pb/^{204}Pb$, both consistent with a higher contribution from a sediment partial melt. The small but significant difference in $^{87}Sr/^{86}Sr$ ratio between Late and Fonualei could then be related to either a fluid with variable $^{87}Sr/^{86}Sr$ ratio due to its multiple origins, as proposed by *Hergt and Woodhead* [2007] or to a sediment partial melt with variable $^{87}Sr/^{86}Sr$ ratio.

[53] The newly acquired Pb isotope data [*Hergt and Woodhead*, 2007; *Pearce et al.*, 2007; this study] combined with the Sr and trace element compositions thus reveal important variations in the nature and origin of the subduction components along the central and south Tonga arc, but also expose the need for extended studies of the different Tonga arc islands and seamounts in order to better comprehend the nature and origin of the subduction components.

4.4. Origin of the Latitudinal Variations

[54] The trace element and isotope variations show that the $^{206}Pb/^{204}Pb$ ratio is the best proxy for the extent of the subduction input to the mantle wedge. The $^{206}Pb/^{204}Pb$ ratio of the southern group, with the exception of four samples, seems to follow a smooth sinusoidal variation (Figure 6). The northern half of sinusoid (21.2–22.8°S), concave downward, is reminiscent of the effect of a circular "plume" interacting with a mid-oceanic ridge [*Schilling*, 1985]. In the southern ELSC case, instead of a mantle plume, the enriched material would be transported by a diapir, with a circular shape and centered where the highest $^{206}Pb/^{204}Pb$ and $^{87}Sr/^{86}Sr$ ratios are observed (~21.55°S) along the spreading center. The wavelength of the sinusoid appears to be ~65 km, which might correspond to the distance between two diapirs reaching the spreading center, a second diapir being located at the southern extremity of VFR1 (~22.2°S). This interval is surprisingly similar to worldwide average spacing between arc volcanoes [*Marsh*, 1979].

[55] The peaks in $^{206}Pb/^{204}Pb$ ratio also correlate with the location of Ata and two submerged volcanoes [*Stoffers et al.*, 2006]. The highest $^{206}Pb/^{204}Pb$ are located above downgoing slab flow lines from Ata, volcano 4 and volcano 3 (Figure 13). A lateral flow from beneath the arc volcanoes toward the ridge would be against the mantle streamlines predicted from corner flow (Figure 14). It is thus more likely that the subduction input observed in the southern ELSC and the south Tonga arc volcanoes reflect a deeper common origin that influences both the volcanic front and the back arc. The weaker $^{206}Pb/^{204}Pb$ peak at 21.9°S could reflect the proximity of volcano 4.

[56] North of the transition C-S, the $^{206}Pb/^{204}Pb$ variation shows that the subduction input to the mantle wedge is more diluted and more diffuse. This may be related to the greater distance from the arc and a decoupling between the arc and back arc. Either the ascending diapirs are assimilated into the

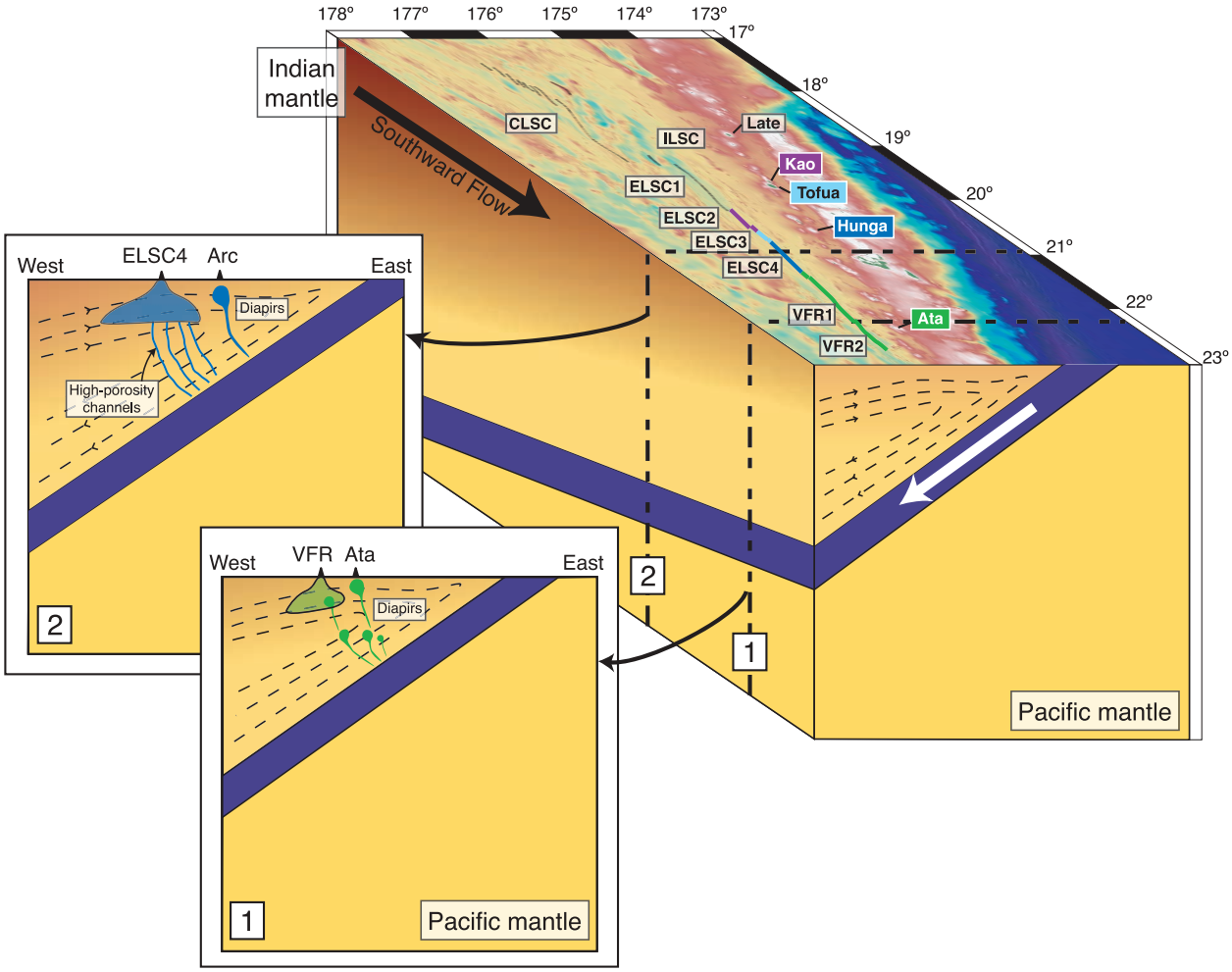

Figure 14. Schematic cartoon illustrating the different processes occurring beneath the Eastern Lau Spreading Center. The replacement of the Pacific-like mantle by an Indian-like mantle is represented by the color gradient. It shows that the Indian signature (brown) increases southward and, for a given latitude, that the deeper mantle has a weaker Indian signature. Different color codes for the name of the Tonga islands and the ELSC ridge reflect the change in subduction-related components. The subduction input beneath Valu Fa (cross section 1) is represented by a diapir which affects the entire melting regime beneath the ridge. The subduction input beneath ELSC4 (cross section 2) is more diffuse along the ridge, possibly reflecting the addition of the subduction input to the melting regime through high-porosity channels.

melting regime at depth or the addition of the subduction input involves another type of transport mechanism such as high-porosity channels.

[57] The abrupt and asymmetrical decrease northward in subduction signature in the northern area (e.g., low $^{206}Pb/^{204}Pb$, Ba/Th and Th/La, Figures 5 and 6), just north of the transition N-C reflects a major change in the basalt petrogenesis. The transition N-C corresponds to the location of the disappearance of the axial magma chamber reflectors beneath the Eastern Lau Spreading Center to the north [*Martinez and Taylor*, 2002] and to the change in ridge morphology from an axial high in the southern ESLC to an axial low in the northern ELSC. The isotope and trace element data show it also reflects an important change of the extent of fluid-rich subduction input to the melting regime. Fluid-enhanced melt productivity in the central and southern ELSC explains both the presence of a magma chamber and the axial high in the southern ELSC. More magma production provides more pathways for extracting melt toward the surface, which could explain the apparent spike of the subduction input just south of the transition N-C, with most of the melt being more efficiently extracted toward the southern part of the transition.

[58] Two samples located within the transition N-C, part of the ELSC3, display a unique chemical

signature: low $^{87}Sr/^{86}Sr$ and high La/Sm possibly reflecting a low-degree melt contribution similar to DR41-1 associated with moderate enrichment in fluid mobile elements. The low-degree melt contribution is consistent with the location of DR41, which is located at the same latitude farther west on the ELSC2, and with the central group located just south of the transition N-C. Deciphering the detailed origin the chemical compositions of these two samples remains difficult because of the major changes in intensity of the two trace element enrichment processes that occur within the transition.

5. Conclusion

[59] Dense sampling of the Eastern Lau Spreading Center reveals that most of the geochemical change along axis occurs within two transitional areas located in the middle of segments. The transitional areas separate geographical provinces with distinctive geochemical characteristics independent of the ridge segmentation. The trace element and isotope variations between these areas reflect the presence of two distinct enrichment processes, one of which is responsible for an E-MORB-like trace element enrichment that has little effect on isotope ratios, and the other for a fluid-dominated enrichment that is variable in composition along axis and is similar to but less intense that what is observed in the Tonga arc lavas. The compositions also reflect the southward migration of Indian-like mantle, progressively replacing the initially Pacific-like mantle wedge.

[60] For most of the ELSC groups, the trace element and isotopic compositions of the subduction end-members can be estimated. The different regions we have defined appear to have distinct subduction inputs with compositions reflecting changes observed in the central and south Tonga arc island lavas. The subduction input of the southern ELSC shows some strong similarities with Ata, the south Tonga island located in its vicinity, while the central ELSC show a subduction input more similar to the central Tonga islands Hunga and Tofua, and the northern ELSC a subduction input similar to Kao (Figure 14). Close to the arc front, the extent of the subduction input to the mantle wedge correlates with the location of the arc volcanoes supporting a coupling between the arc and the back arc. Further from the arc front, the distribution of the subduction input is more diffuse. This likely reflects a different depth of origin and a different mechanism of transport for the subduction input than for the arc.

[61] The combination of the back-arc and arc data allows identification of the involvement of several components contributing to the subduction input. Overall, the subduction input is composed of a fluid (derived from the altered oceanic crust with a possible sedimentary contribution) and a sediment partial melt. In Ata and possibly the southern part of the central Tonga islands, volcaniclastic sediments associated with the subducted Lousiville Seamount Chain contribute significantly to the subduction input. Farther north, the central Tonga Islands do not have such a contribution. While on a regional scale there is a decrease in subduction influence with the distance from the arc, on a small scale, the distribution of the subduction input is not directly related to the distance from the arc front. It rather reflects the mechanisms of the addition of the subduction input to the mantle wedge.

[62] Knowing the subduction input compositions permits an estimate of the mantle wedge composition for the different groups. Our data set confirms a progressively stronger Indian-like signature toward the north for the mantle wedge. This observation supports a southward flow of Indian-like mantle, likely associated with the basin opening, as illustrated in Figure 14. The estimated mantle wedge composition for the southern ELSC has a less Indian-like signature than farther north but does not display a Pacific-like signature comparable to the ODP Sites 834 and 839 [*Ewart et al.*, 1994b; *Hergt and Farley*, 1994; *Hergt and Hawkesworth*, 1994; *Ewart et al.*, 1998]. The initially Pacific-like mantle appears to have been mostly replaced.

[63] Our data set also reveals the existence of an E-MORB-like trace element enrichment that occurs prior to the subduction input, without affecting significantly the isotopic compositions. This enrichment has the strongest effect on the composition of sample DR41-1. It reflects the preconditioning of the mantle wedge by a low-degree melt derived from a deeper part of the mantle which has a slightly less Indian-like isotopic signature.

Appendix A: Analytical Methods

[64] Pb, Sr, and Nd chemical extractions were performed at Harvard except for the Sr duplicates of RC067 and RC069 done at LDEO. The isotope ratios were measured at LDEO. Within every batch, DR41-1 was dissolved at least once. The compilation of DR41-1 data gives an estimate of

Table A1. Compositions of the Rock Standards Used for the Trace Element Calibration Curves[a]

	Sr	La	Ce	Nd	Sm	Nb	Ba	Pb	Th	U
BHVO-2	388	15	36.8	24.20	5.92	19.80	129	1.66	1.19	0.412
DNC-1	144.5	3.56	8.3	4.98	1.43	1.66	103	6.30	0.24	0.05
W2	196.5	10.7	23.4	12.91	3.24	7.90	172	7.80	2.10	0.49
JB-2	178	2.4	6.64	6.70	2.25	0.57	218	5.31	0.26	0.15
MAR	92	2.02	6.94	7.60	2.715	1.534	6.6	0.31	0.096	0.075

[a] Unit is ppm.

the external reproducibility on our analyses after standard normalization.

[65] Pb and Sr isotope ratios were measured on a Micromass Sector 54 thermal ionization mass spectrometer at LDEO. Pb isotope ratios were determined using a ^{207}Pb-^{204}Pb double spike. SRM981 was analyzed every few samples and used to correct the measured values to ^{206}Pb/^{204}Pb = 16.9356, ^{207}Pb/^{204}Pb = 15.4891, and ^{208}Pb/^{204}Pb = 36.7006 [*Todt et al.*, 1996]. Reproducibility for SRM981 is 412, 570, and 577 ppm (2σ, N = 36), for ^{206}Pb/^{204}Pb, ^{207}Pb/^{204}Pb, and ^{208}Pb/^{204}Pb ratios, respectively. After filtering out measurements outside of 2σ from the mean value, the reproducibility is 338, 416, and 470 ppm, respectively. Reproducibility for DR41-1 is 478, 443, and 561 ppm (2σ, N = 11), for ^{206}Pb/^{204}Pb, ^{207}Pb/^{204}Pb, and ^{208}Pb/^{204}Pb ratios, respectively.

[66] Sr isotopic measurements were performed with typical ^{88}Sr beam intensities of 5×10^{-11} amps. ^{87}Sr/^{86}Sr ratios were normalized to ^{86}Sr/^{88}Sr = 0.1194. SRM987 was analyzed every few samples and used to correct the measured sample values to ^{87}Sr/^{86}Sr = 0.710235. Before normalization. SRM987 measurements average to 0.710277 ± 0.000023 (N = 47). After filtering out measurements outside of 2σ from the mean value, the average is 0.710274 ± 0.000019. Reproducibility for DR41-1 is 36 ppm (0.703042 ± 0.000025 (2σ; N = 16)).

[67] ^{143}Nd/^{144}Nd ratios were measured on an Axiom multicollector ICP-MS at LDEO and normalized to ^{146}Nd/^{144}Nd = 0.7219, with typical ^{144}Nd beam intensities from 2 to 4 Volts. Samples were bracketed by JNdi (200ppb solution) and ^{143}Nd/^{144}Nd ratios corrected to a value of 0.512115 for JNdi-1 [*Tanaka et al.*, 2000]. While JNdi daily averages were variable because of different tuning conditions and outside factors, typical reproducibility on ^{143}Nd/^{144}Nd ratios is 35 ppm (±0.000018). After correction using the bracketing standards, the external reproducibility for DR41-1 is 24 ppm (0.513018 ± 0.000012 (2σ; N = 23)). For this study, several samples were measured twice, and the reproducibility obtained was consistent with the one for DR41-1.

[68] Trace element concentrations were determined using a Thermo X-series ICP-MS quadripole at Harvard University. The samples were processed using the method described in A. Bezos et al. (Origins of chemical diversity of back-arc basin basalts: A segment-scale study of the northern Eastern Lau Spreading Center, submitted to *Journal of Geophysical Research*, 2008). ^{72}Ge, ^{103}Rh, ^{115}In, ^{169}Tm, and ^{209}Bi were used for internal standard normalization. Our in-house standard K1919 was used for drift correction and BHVO-2, W2, DNC-1, JB-2 and MAR were used for the calibration curves (see Table A1).

[69] Major element compositions were performed on glassy pillow rim material using the JEOL JXA-733 electron microprobe at MIT and normalized to the VE32 glass standard. For more details, please refer to Bezos et al. (submitted manuscript, 2008).

Appendix B: Comparison With Existing Tonga and Valu Pb Isotopic Data

[70] As recently pointed out by *Hergt and Woodhead* [2007], there are significant differences between the Pb isotopes ratios reported for the same samples in earlier studies of the Tonga arc, especially between *Ewart et al.* [1998] (which includes data from *Regelous et al.* [1997]), and *Turner et al.* [1997]. *Hergt and Woodhead* [2007] reported new Pb data for 14 samples previously analyzed by *Ewart et al.* [1998], 7 of which have been also analyzed by *Turner et al.* [1997]. To summarize, their new data show the same range of variation as the *Ewart et al.* [1998] data for ^{206}Pb/^{204}Pb and ^{208}Pb/^{204}Pb but a significant offset toward lower ^{207}Pb/^{204}Pb (Figure B1). When compared to the new *Hergt and Woodhead* [2007] data, *Turner et al.* [1997] data appear to be significantly shifted toward lower ^{206}Pb/^{204}Pb and ^{208}Pb/^{204}Pb, and show substantial variability in

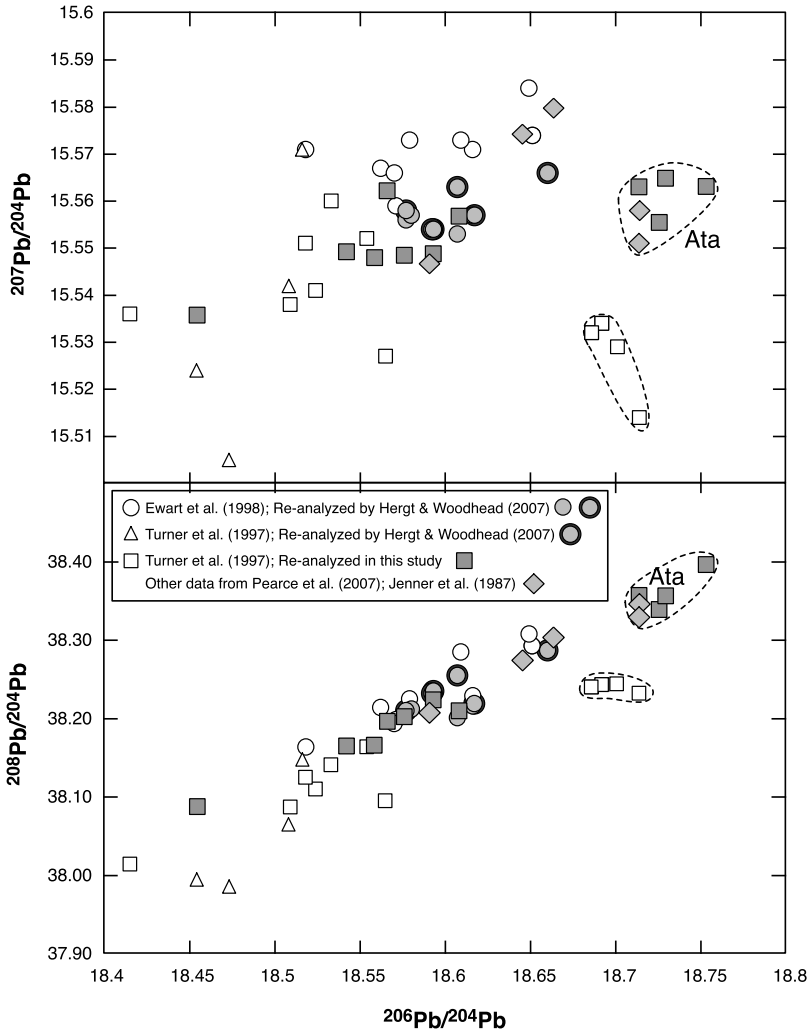

Figure B1. Comparison of the recent and other Pb data. Note that the gray circles with the black contours represent samples analyzed by both *Turner et al.* [1997] and *Ewart et al.* [1998] and reanalyzed by *Hergt and Woodhead* [2007].

$^{207}Pb/^{204}Pb$ for the $^{206}Pb/^{204}Pb$ range. For a more detailed discussion on the possible origins of the Pb ratio discrepancies, the reader is referred to *Hergt and Woodhead* [2007]. On the basis of their new data set, *Hergt and Woodhead* [2007, p. 23] concluded that the older data "appear to be inappropriate to address current issues in arc geochemistry and should be superseded by the data obtained with modern methods and instrumentation."

[71] In order to better constrain the nature of the subduction component(s) affecting the mantle beneath the Eastern Lau Spreading Center, we need to be able to compare our new data set with the central and south Tonga arc islands (from north to south: Fonualei, Late, Tofua, Kao, and Ata). Only one other recent study of the Tonga arc reported new Pb isotopic ratios [*Pearce et al.*, 2007]. *Pearce et al.* [2007] have analyzed a total of 4 new samples from 4 different islands (Ata, Tofua, Hunga A'apai and Late). Combined, the two recent studies [*Hergt and Woodhead*, 2007; *Pearce et al.*, 2007] provide new Pb isotopic compositions for three samples each from Kao, Late, Hunga A'apai, and Fonualei, but only one each for Tofua and Ata.

[72] We report new Pb isotopic data for 4 samples from Ata, 3 from Tofua, 3 from Late and 3 from Fonualei, which have almost all been previously analyzed by *Turner et al.* [1997]. Our new Pb compositions confirm the shift toward lower $^{206}Pb/^{204}Pb$, $^{207}Pb/^{204}Pb$ and $^{208}Pb/^{204}Pb$ ratios for *Turner et al.* [1997] data compared to the recent analyses (Figure B1). Our new Pb ratios for Ata lavas are consistent with the analysis made by

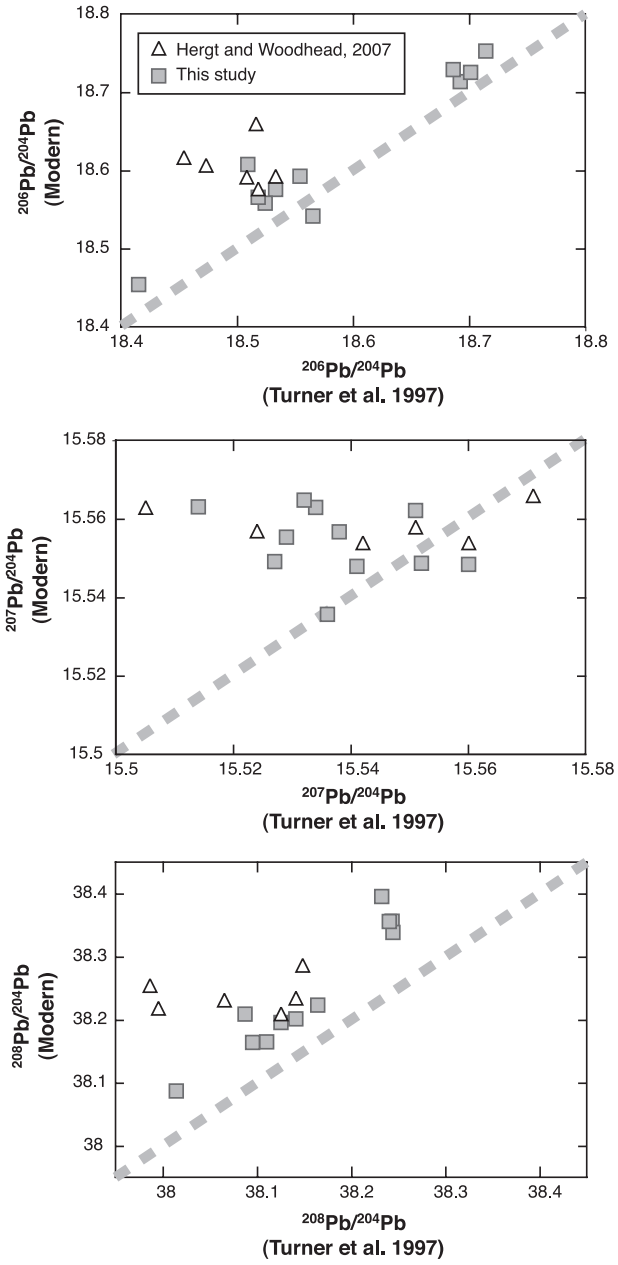

Figure B2. Comparison of Pb ratios: *Turner et al.* [1997] versus *Hergt and Woodhead* [2007] and this study.

Pearce et al. [2007], which is an expected result since they also use NBS981 as a standard (Figure B2). Our analyses area also in agreement with the analysis made by *Jenner et al.* [1987], confirming the absence of a bias between their data and recent data. These six compositions of Ata lavas confirm the existence of a $^{207}Pb/^{204}Pb$ offset relative to the central Tonga Island trend, with little if any offset in $^{208}Pb/^{204}Pb$ (Figure B1). For Tofua, while having slightly higher Pb isotopic ratios compared to *Turner et al.* [1997] data for the same samples, our new data together with the *Pearce et al.* [2007] data confirm the significant range of Pb isotopic ratios, ranging from 18.454 (instead of 18.415) to 18.645. Kao, Late and Fonualei lavas have a smaller range of variation of Pb isotope ratios within the range for Tofua lavas.

[73] The comparison of the more recent data from the central and south Tonga arc islands with either *Turner et al.* [1997] or *Ewart et al.* [1998] data does not provide any simple relationship that may allow for correction of their data. Like *Hergt and Woodhead* [2007], we conclude that the more recent Pb analyses should be used to discuss the origin of the arc geochemical variability and for comparison with our new data set for the Eastern Lau Spreading Center.

[74] Only one sample has been analyzed by both *Hergt and Woodhead* [2007] and us and there is a small offset ($^{206}Pb/^{204}Pb$: 18.577 versus 18.566, $^{207}Pb/^{204}Pb$: 15.558 versus 15.562 and $^{208}Pb/^{204}Pb$: 38.21 versus 38.196, for *Hergt and Woodhead* [2007] and us, respectively) which does not seem to be significant compared to the offset with the older data. In order to be sure of the absence of bias between the recent data, we report in Figure B2 the comparison between the old *Turner et al.* [1997] data and the recent data. For the $^{206}Pb/^{204}Pb$ and $^{208}Pb/^{204}Pb$ ratios, our data define a trend parallel to the 1:1 line, offset toward higher values. For the $^{207}Pb/^{204}Pb$ ratio, our data show less variability than the *Turner et al.* [1997] data but no systematic offset. The *Hergt and Woodhead* [2007] data display significantly less variation than the data obtained on the same samples by *Turner et al.* [1997]. The offset from the 1:1 line is higher for the *Hergt and Woodhead* [2007] data than for ours, suggesting a possible analytical bias.

[75] In this study, we chose not to include the existing Pb isotope data obtained on Valu Fa samples [*Loock et al.*, 1990; *Loock*, 1992]. As illustrated in Figure B3, most of the $^{207}Pb/^{204}Pb$ ratios from these analyses are offset toward higher values.

Appendix C: References for the Data Used in Figures 1, 2, 4, and 7–12

[76] In Figure 1, the locations of the CLSC, ILSC and other ELSC samples are from *Sunkel* [1990], *Falloon et al.* [1992], *Volpe et al.* [1988], *Loock* [1992], *Pearce et al.* [1995], *Peate et al.* [2001],

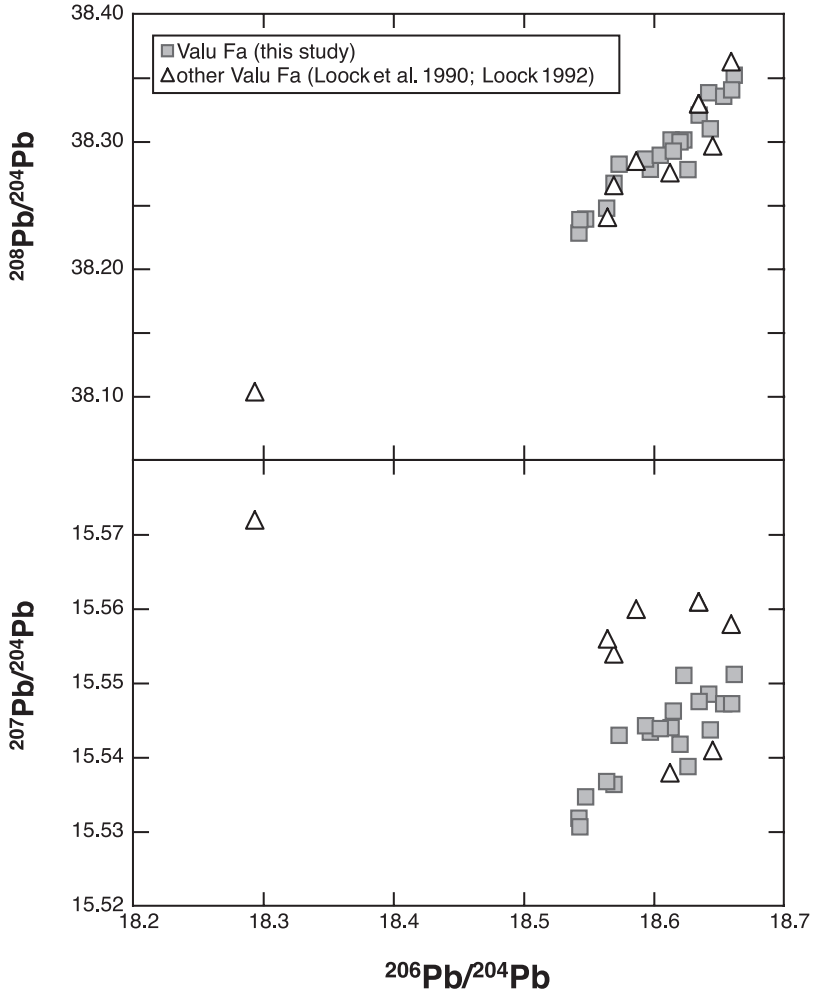

Figure B3. Comparison of the published Pb data for Valu Fa to our new Pb data.

and *Hergt and Woodhead* [2007]. ODP site locations are from *Hawkins and Allan* [1994].

[77] In Figure 2, data for the Lau basin are from *Sunkel* [1990], *Falloon et al.* [1992], *Loock* [1992], *Danyushevsky et al.* [1993], *Pearce et al.* [1995], *Kamenetsky et al.* [1997], *Peate et al.* [2001], and *Pearce et al.* [2007]. Data for the East Scotia basin are from *Leat et al.* [2000] and *Fretzdorff et al.* [2002]. Data for the Manus basin are from *Sinton et al.* [2003]. Data for the Mariana Trough are from *Sinton and Fryer* [1987], *Hawkins et al.* [1990], *Volpe et al.* [1990], *Gribble et al.* [1996, 1998], *Peate and Pearce* [1998], *Leat et al.* [2004], and *Pearce et al.* [2005]. Samoa Island data are from *Palacz and Saunders* [1986], *Wright and White* [1987], *Farley et al.* [1992], and *Workman et al.* [2004]. CLSC and ELSC data are from this study and a compiled file from PetDB [*Pearce et al.*, 1995; *Peate et al.*, 2001; *Pearce et al.*, 2007].

[78] In Figure 4, CLSC and ELSC1 data are from a compiled file from PetDB [*Pearce et al.*, 1995; *Peate et al.*, 2001; *Pearce et al.*, 2007]. Tonga arc data (only the recent Pb data are reported) are from this study and *Turner et al.* [1997], *Ewart et al.* [1998], *Hergt and Woodhead* [2007], and *Pearce et al.* [2007]. Louisville Seamount Chain data are from *Cheng et al.* [1987] and *Hawkins et al.* [1987]. Samoa Island data are from *Palacz and Saunders* [1986], *Wright and White* [1987], *Farley et al.* [1992], and *Workman et al.* [2004]. Pelagic and volcaniclastic sediments (site 204) data are from *Turner et al.* [1997] and *Ewart et al.* [1998]. CIR data are from S. Escrig (unpublished trace element data, 2008) and a compiled file from PetDB [*Dupré and Allègre*, 1983; *Mahoney et al.*, 1989; *Rehkämper and Hofmann*, 1997; *Escrig et al.*, 2004; *Nauret et al.*, 2006]. EPR data are from a compiled file from PetDB [*Batiza and Johnson*, 1980; *Sun*, 1980; *Vidal and Clauer*, 1981; *Batiza et al.*, 1982; *Macdougall and Lugmair*, 1986; *Ito et*

al., 1987; *White et al.*, 1987; *Prinzhofer et al.*, 1989; *Mahoney et al.*, 1994; *Bach et al.*, 1994; *Harpp*, 1995; *Niu et al.*, 1996; *Schiano et al.*, 1997; *Nowell et al.*, 1998; *Niu et al.*, 1999; *Regelous et al.*, 1999; *Castillo et al.*, 2000; *Chauvel and Blichert-Toft*, 2001; *Haase*, 2002].

[79] In Figure 7, CLSC and ELSC1 data are from a compiled file from PetDB [*Pearce et al.*, 1995; *Peate et al.*, 2001; *Pearce et al.*, 2007]. East Pacific Rise ICP-MS trace element data are from a compiled file from PetDB [*Harpp*, 1995; *Schiano et al.*, 1997; *Niu et al.*, 1999; *Regelous et al.*, 1999; *Chauvel and Blichert-Toft*, 2001; *Haase*, 2002].

[80] In Figure 8, CLSC and ELSC1 data are from a compiled file from PetDB [*Pearce et al.*, 1995; *Peate et al.*, 2001; *Pearce et al.*, 2007]. Tonga arc data are from *Turner et al.* [1997], *Ewart et al.* [1998], *Hergt and Woodhead* [2007], and *Pearce et al.* [2007]. EPR ICP-MS trace element and isotope data are from a compiled file from PetDB [*Batiza and Johnson*, 1980; *Sun*, 1980; *Vidal and Clauer*, 1981; *Batiza et al.*, 1982; *Macdougall and Lugmair*, 1986; *Ito et al.*, 1987; *White et al.*, 1987; *Prinzhofer et al.*, 1989; *Mahoney et al.*, 1994; *Bach et al.*, 1994; *Harpp*, 1995; *Niu et al.*, 1996; *Schiano et al.*, 1997; *Nowell et al.*, 1998; *Niu et al.*, 1999; *Regelous et al.*, 1999; *Castillo et al.*, 2000; *Chauvel and Blichert-Toft*, 2001; *Haase*, 2002]. CIR data are from S. Escrig (unpublished trace element data, 2008) and a compiled file from PetDB [*Dupré and Allègre*, 1983; *Mahoney et al.*, 1989; *Rehkämper and Hofmann*, 1997; *Escrig et al.*, 2004; *Nauret et al.*, 2006].

[81] In Figure 9, CLSC and ELSC1 data are from a compiled file from PetDB [*Pearce et al.*, 1995; *Peate et al.*, 2001; *Pearce et al.*, 2007]. Tonga arc data (only the recent Pb data are reported) are from this study and *Jenner et al.* [1987], *Turner et al.* [1997], *Ewart et al.* [1998], *Hergt and Woodhead* [2007], and *Pearce et al.* [2007].

[82] In Figure 10, CLSC and ELSC1 data are from a compiled file from PetDB [*Pearce et al.*, 1995; *Peate et al.*, 2001; *Pearce et al.*, 2007]. Tonga arc data are from this study and *Turner et al.* [1997], *Ewart et al.* [1998], *Hergt and Woodhead* [2007], and *Pearce et al.* [2007]. EPR ICP-MS trace element and isotope data are from a compiled file from PetDB [*Batiza and Johnson*, 1980; *Sun*, 1980; *Vidal and Clauer*, 1981; *Batiza et al.*, 1982; *Macdougall and Lugmair*, 1986; *Ito et al.*, 1987; *White et al.*, 1987; *Prinzhofer et al.*, 1989; *Mahoney et al.*, 1994; *Bach et al.*, 1994; *Harpp*, 1995; *Niu et al.*, 1996; *Schiano et al.*, 1997; *Nowell et al.*, 1998; *Niu et al.*, 1999; *Regelous et al.*, 1999; *Castillo et al.*, 2000; *Chauvel and Blichert-Toft*, 2001; *Haase*, 2002]. CIR data are from S. Escrig (unpublished trace element data, 2008) and a compiled file from PetDB [*Dupré and Allègre*, 1983; *Mahoney et al.*, 1989; *Rehkämper and Hofmann*, 1997; *Escrig et al.*, 2004; *Nauret et al.*, 2006].

[83] In Figure 11, CLSC and ELSC1 data are from a compiled file from PetDB [*Pearce et al.*, 1995; *Peate et al.*, 2001; *Pearce et al.*, 2007]. Tonga arc data are from this study and *Jenner et al.* [1987], *Turner et al.* [1997], *Ewart et al.* [1998], *Hergt and Woodhead* [2007], and *Pearce et al.* [2007]. EPR ICP-MS trace element and isotope data are from a compiled file from PetDB [*Batiza and Johnson*, 1980; *Sun*, 1980; *Vidal and Clauer*, 1981; *Batiza et al.*, 1982; *Macdougall and Lugmair*, 1986; *Ito et al.*, 1987; *White et al.*, 1987; *Prinzhofer et al.*, 1989; *Mahoney et al.*, 1994; *Bach et al.*, 1994; *Harpp*, 1995; *Niu et al.*, 1996; *Schiano et al.*, 1997; *Nowell et al.*, 1998; *Niu et al.*, 1999; *Regelous et al.*, 1999; *Castillo et al.*, 2000; *Chauvel and Blichert-Toft*, 2001; *Haase*, 2002]. Tonga arc data are from this study and *Turner et al.* [1997], *Ewart et al.* [1998], *Hergt and Woodhead* [2007], and *Pearce et al.* [2007]. CIR data are from S. Escrig (unpublished trace element data, 2008) and *Dupré and Allègre* [1983], *Mahoney et al.* [1989], *Rehkämper and Hofmann* [1997], *Escrig et al.* [2004], and *Nauret et al.* [2006]. Louisville Seamount Chain data are from *Cheng et al.* [1987] and *Hawkins et al.* [1987]. Samoa Island data are from *Palacz and Saunders* [1986], *Wright and White* [1987], *Farley et al.* [1992], and *Workman et al.* [2004]. Pelagic and volcaniclastic sediments (site 204) data are from *Turner et al.* [1997] and *Ewart et al.* [1998].

[84] In Figure 12, CLSC and ELSC data are from this study and a compiled file from PetDB [*Pearce et al.*, 1995; *Peate et al.*, 2001; *Pearce et al.*, 2007]. Tonga arc data are from this study and *Turner et al.* [1997], *Ewart et al.* [1998], *Hergt and Woodhead* [2007], and *Pearce et al.* [2007]. EPR ICP-MS trace element and isotope data are from *Batiza and Johnson* [1980], *Sun* [1980], *Vidal and Clauer* [1981], *Batiza et al.* [1982], *Macdougall and Lugmair* [1986], *Ito et al.* [1987], *White et al.* [1987], *Prinzhofer et al.* [1989], *Mahoney et al.* [1994], *Bach et al.* [1994], *Harpp* [1995], *Niu et al.* [1996], *Schiano et al.* [1997], *Nowell et al.*

[1998], *Niu et al.* [1999], *Regelous et al.* [1999], *Castillo et al.* [2000], *Chauvel and Blichert-Toft* [2001], and *Haase* [2002]. Tonga arc data are from this study and *Jenner et al.* [1987], *Turner et al.* [1997], *Ewart et al.* [1998], *Hergt and Woodhead* [2007], and *Pearce et al.* [2007]. Louisville Seamount Chain data are from *Cheng et al.* [1987] and *Hawkins et al.* [1987]. Pelagic and volcaniclastic sediments (site 204) data are from *Turner et al.* [1997] and *Ewart et al.* [1998]. ODP site 834 data are from *Hergt and Farley* [1994].

Acknowledgments

[85] We thank A. Cipriani, Y. Cai, and T. van de Flierdt for assistance with isotope analyses at LDEO. Comments by V. Salters, K. Kelley, and an anonymous reviewer greatly helped to improve the manuscript. This work was supported by the National Science Foundation (OCE-0242618 and OCE 0242675).

References

Allègre, C. J. (1987), Isotope geodynamics, *Earth Planet. Sci. Lett.*, *86*, 175–203, doi:10.1016/0012-821X(87)90220-2.

Bach, W., E. Hegner, J. Erzinger, and M. Satir (1994), Chemical and isotopic variations along the superfast spreading East Pacific Rise from 6°S to 30°S, *Contrib. Mineral. Petrol.*, *116*, 365–380.

Batiza, R., and J. R. Johnson (1980), Trace element and isotopic evidence for magma mixing in alkalic and transitional basalts near the East Pacific Rise at 8°N, *Initial Rep. Deep Sea Drill. Proj.*, *54*, 63–69.

Batiza, R., R. Oestrike, and K. Futa (1982), Chemical and isotopic diversity in basalts dredged from the East Pacific Rise at 10°C, the fossil Galapagos Rise and the Nazca plate, *Mar. Geol.*, *49*, 115–132, doi:10.1016/0025-3227(82)90032-9.

Bevis, M., et al. (1995), Geodetic observations of very rapid convergence and back-arc extension at the Tonga arc, *Nature*, *374*, 249–251, doi:10.1038/374249a0.

Castillo, P. R., E. M. Klein, J. F. Bender, C. H. Langmuir, S. B. Shirey, R. Batiza, and W. M. White (2000), Petrology and Sr, Nd, and Pb isotope geochemistry of mid-ocean ridge basalt glasses from the 11°45′N to 15°00′N segment of the East Pacific Rise, *Geochem. Geophys. Geosyst.*, *1*(11), 1011, doi:10.1029/1999GC000024.

Chauvel, C., and J. Blichert-Toft (2001), A hafnium isotope and trace element perspective on melting of the depleted mantle, *Earth Planet. Sci. Lett.*, *190*, 137–151, doi:10.1016/S0012-821X(01)00379-X.

Cheng, Q., K.-H. Park, J. D. MacDougall, A. Zindler, G. W. Lugmair, H. Staudigel, J. Hawkins, and P. Lonsdale (1987), Isotopic evidence for a hotspot origin of the Louisville Seamount chain, in *Seamounts, Islands, and Atolls*, *Geophys. Monogr. Ser.*, vol. 43, edited by B. H. Keating et al., pp. 283–296, AGU, Washington, D. C.

Conder, J. A., D. A. Wiens, and J. D. Morris (2002), On the decompression melting structure at volcanic arcs and back-arc spreading centers, *Geophys. Res. Lett.*, *29*(15), 1727, doi:10.1029/2002GL015390.

Danyushevsky, L. V., T. J. Falloon, A. V. Sobolev, A. J. Crawford, M. Carroll, and R. C. Price (1993), The H_2O content of basalt glasses from southwest Pacific back-arc basins, *Earth Planet. Sci. Lett.*, *117*, 347–362, doi:10.1016/0012-821X(93)90089-R.

Donnelly, K. E., S. L. Goldstein, C. H. Langmuir, and M. Spiegelman (2004), Origin of enriched ocean ridge basalts and implications for mantle dynamics, *Earth Planet. Sci. Lett.*, *226*, 347–366, doi:10.1016/j.epsl.2004.07.019.

Dupré, B., and C. J. Allègre (1983), Pb-Sr isotope variation in Indian Ocean basalts and mixing phenomena, *Nature*, *303*, 142–146, doi:10.1038/303142a0.

Escrig, S., F. Capmas, B. Dupré, and C. J. Allègre (2004), Osmium isotopic constraints on the nature of the DUPAL anomaly from Indian mid-ocean-ridge basalts, *Nature*, *431*, 59–63, doi:10.1038/nature02904.

Ewart, A., W. B. Bryan, B. W. Chappell, and R. L. Rudnick (1994a), Regional geochemistry of the Lau-Tonga arc and backarc systems*Proc. Ocean Drill. Program Sci. Results*, *135*, 385–425.

Ewart, A., J. M. Hergt, and J. W. Hawkins (1994b), Major element, trace element, and isotope (Pb, Sr, and Nd) geochemistry of site 839 basalts and basaltic andesites: Implications for arc volcanism, *Proc. Ocean Drill. Program Sci. Results*, *135*, 519–531.

Ewart, A., K. D. Collerson, M. Regelous, J. I. Wendt, and Y. Niu (1998), Geochemical evolution within the Tonga-Kermadec Lau arc back-arc systems: The role of varying mantle wedge composition in space and time, *J. Petrol.*, *39*, 331–368, doi:10.1093/petrology/39.3.331.

Falloon, T. J., A. Malahoff, L. P. Zonenshain, and Y. Bogdanov (1992), Petrology and geochemistry of back-arc basin basalts from Lau basin spreading ridges at 15, 18, and 19°S, *Mineral. Petrol.*, *47*, 1–35, doi:10.1007/BF01165295.

Farley, K., J. Natland, and H. Craig (1992), Binary mixing of enriched and undegassed (primitive?) mantle components (He, Sr, Nd, Pb) in Samoan lavas, *Earth Planet. Sci. Lett.*, *111*, 183–199, doi:10.1016/0012-821X(92)90178-X.

Fretzdorff, S., R. A. Livermore, C. W. Devey, P. T. Leat, and P. Stoffers (2002), Petrogenesis of the back-arc east Scotia Ridge, South Atlantic Ocean, *J. Petrol.*, *43*, 1435–1467, doi:10.1093/petrology/43.8.1435.

Gribble, R. F., R. J. Stern, S. H. Bloomer, D. Stuben, T. O'Hearn, and S. Newman (1996), MORB mantle and subduction components interact to generate basalts in the southern Mariana Trough back-arc basin, *Geochim. Cosmochim. Acta*, *60*, 2153–2166, doi:10.1016/0016-7037(96)00078-6.

Gribble, R. F., R. J. Stern, S. Newman, S. H. Bloomer, and T. O'Hearn (1998), Chemical and isotopic composition of lavas from the Northern Mariana Trough: Implications for magmagenesis in back-arc basins, *J. Petrol.*, *39*, 125–154, doi:10.1093/petrology/39.1.125.

Haase, K. M. (2002), Geochemical constraints on magma sources and mixing processes in Easter Microplate MORB (SE Pacific): A case study of plume-ridge interaction, *Chem. Geol.*, *182*, 335–355, doi:10.1016/S0009-2541(01)00327-8.

Harding, A. J., G. M. Kent, and J. A. Collins (2000), Initial results from a multichannel seismic survey of the Lau back-arc basin, *Eos Trans. AGU*, *81*(48), Fall Meet. Suppl., Abstract T61C-16.

Harpp, K. S. (1995), Geochemical variations in a single basaltic flow at 9°30′N on the East Pacific Rise, *Proc. Ocean Drill. Program Sci. Results*, *142*, 9–22.

Hart, S. R. (1984), A large-scale isotope anomaly in the Southern Hemisphere mantle, *Nature*, *309*, 753–757, doi:10.1038/309753a0.

Hart, S. R. (1988), Heterogeneous mantle domains: Signatures, genesis and mixing chronologies, *Earth Planet. Sci. Lett.*, *90*, 273–296, doi:10.1016/0012-821X(88)90131-8.

Hawkesworth, C. J., N. W. Rogers, P. W. Van Calsteren, and M. A. Menzies (1984), Mantle enrichment processes, *Nature*, *311*, 331–335, doi:10.1038/311331a0.

Hawkins, J. W., and J. F. Allan (1994), Petrologic evolution of the Lau basin, sites 834–839, *Proc. Ocean Drill. Program Sci. Results*, *135*, 427–470.

Hawkins, J. W., P. F. Lonsdale, and R. Batiza (1987), Petrologic evolution of the Louisville seamount chain, in *Seamounts, Islands, and Atolls*, *Geophys. Monogr. Ser.*, vol. 43, edited by B. Keating et al., pp. 235–254, AGU, Washington, D. C.

Hawkins, J. W., P. F. Lonsdale, J. D. Macdougall, and A. M. Volpe (1990), Petrology of the axial ridge of the Mariana Trough backarc spreading center, *Earth Planet. Sci. Lett.*, *100*, 226–250.

Hergt, J. M., and K. N. Farley (1994), Major element, trace element, and isotope (Pb, Sr, and Nd) variations in Site 834 basalts: Implications for the initiation of backarc opening, *Proc. Ocean Drill. Program Sci. Results*, *135*, 471–485.

Hergt, J. M., and C. J. Hawkesworth (1994), Pb, Sr and Nd isotopic evolution of the Lau basin: Implications for mantle dynamics during backarc opening, *Proc. Ocean Drill. Program Sci. Results*, *135*, 505–517.

Hergt, J. M., and J. D. Woodhead (2007), A critical evaluation of recent models for Lau-Tonga arc-backarc basin magmatic evolution, *Chem. Geol.*, *245*, 9–44, doi:10.1016/j.chemgeo.2007.07.022.

Hofmann, A. W., and W. M. White (1982), Mantle plumes from ancient oceanic crust, *Earth Planet. Sci. Lett.*, *57*, 421–436, doi:10.1016/0012-821X(82)90161-3.

Ito, E., W. M. White, and C. Gopel (1987), The O, Sr, Nd and Pb isotope geochemistry of MORB, *Chem. Geol.*, *62*, 157–176, doi:10.1016/0009-2541(87)90083-0.

Jacobs, A. M., A. J. Harding, and G. H. Kent (2007), Axial crustal structure of the Lau back-arc basin from velocity modeling of multichannel seismic data, *Earth Planet. Sci. Lett.*, *259*, 239–255, doi:10.1016/j.epsl.2007.04.021.

Jenner, G. A., P. A. Cawood, M. Rautenschlein, and W. M. White (1987), Composition of back-arc basin volcanics, Valu Fa ridge, Lau basin: Evidence for a slab-derived component in their mantle source, *J. Volcanol. Geotherm. Res.*, *32*, 209–222, doi:10.1016/0377-0273(87)90045-X.

Kamenetsky, V. S., A. J. Crawford, S. Eggins, and R. Muhe (1997), Phenocryst and melt inclusion chemistry of near-axis seamounts, Valu Fa Ridge, Lau basin: Insight into mantle wedge melting and the addition of subduction components, *Earth Planet. Sci. Lett.*, *151*, 205–223, doi:10.1016/S0012-821X(97)81849-3.

Karig, D. E. (1970), Ridges and basins of Tonga-Kermadec island arc system, *J. Geophys. Res.*, *75*, 239–254, doi:10.1029/JB075i002p00239.

Kelley, K. A., T. Plank, T. L. Grove, E. M. Stolper, S. Newman, and E. H. Hauri (2006), Mantle melting as a function of water content beneath back-arc basins, *J. Geophys. Res.*, *111*, B09208, doi:10.1029/2005JB003732.

Langmuir, C. H., A. Bezos, S. Escrig, and S. W. Parman (2006), Chemical systematics and hydrous melting of the mantle in back-arc basins, in *Back-Arc Spreading Systems: Geological, Biological, Chemical, and Physical Interactions*, *Geophys. Monogr. Ser.*, vol. 166, edited by D. M. Christie et al., pp. 87–146, AGU, Washington, D. C.

Leat, P. T., R. A. Livermore, I. L. Millar, and J. A. Pearce (2000), Magma supply in back-arc spreading centre segment E2, east Scotia Ridge, *J. Petrol.*, *41*, 845–866, doi:10.1093/petrology/41.6.845.

Leat, P. T., J. A. Pearce, P. F. Barker, I. L. Millar, T. L. Barry, and R. D. Larter (2004), Magma genesis and mantle flow at a subducting slab edge: The South Sandwich arc-basin system, *Earth Planet. Sci. Lett.*, *227*, 17–35, doi:10.1016/j.epsl.2004.08.016.

Loock, G. (1992), Character and distribution of the Indian Ocean domain: A study of the mantle source compositions of Lau basin volcanics (SW Pacific) and the Indian Ocean mid-oceanic ridge basalts, Ph.D. thesis, Univ. zu Köln, Cologne, Germany.

Loock, G., W. F. McDonough, S. L. Goldstein, and A. W. Hofmann (1990), Isotopic compositions of volcanic glasses from the Lau basin, *Mar. Geol.*, *9*, 235–245.

Macdougall, J. D., and G. W. Lugmair (1986), Sr and Nd isotopes in basalts from the East Pacific Rise—Significance for mantle heterogeneity, *Earth Planet. Sci. Lett.*, *77*, 273–284, doi:10.1016/0012-821X(86)90139-1.

Mahoney, J. J., J. H. Natland, W. M. White, R. Poreda, S. H. Bloomer, R. L. Fishe, and A. N. Baxter (1989), Isotopic and geochemical provinces of the western Indian Ocean spreading centers, *J. Geophys. Res.*, *94*, 4033–4052, doi:10.1029/JB094iB04p04033.

Mahoney, J. J., J. M. Sinton, M. D. Kurz, J. D. MacDougall, K. J. Spencer, and G. W. Lugmair (1994), Isotope and trace element characteristics of a super-fast spreading ridge: East Pacific Rise, 13–23°S, *Earth Planet. Sci. Lett.*, *121*, 173–193, doi:10.1016/0012-821X(94)90039-6.

Marsh, B. D. (1979), Island-arc volcanism, *Am. Sci.*, *67*, 161–172.

Martinez, F., and B. Taylor (2002), Mantle wedge control on back-arc crustal accretion, *Nature*, *416*, 417–420.

Nauret, F., W. Abouchami, S. J. G. Galer, A. W. Hoffmann, C. Hémond, C. Chauvel, and J. Dyment (2006), Correlated trace element-Pb isotope enrichments in Indian MORB along 18–20°S, central Indian Ridge, *Earth Planet. Sci. Lett.*, *245*, 137–152, doi:10.1016/j.epsl.2006.03.015.

Niu, Y., D. Waggoner, J. Sinton, and J. Mahoney (1996), Mantle source heterogeneity and melting processes beneath seafloor spreading centers: The East Pacific Rise, 18°–19°S, *J. Geophys. Res.*, *101*, 27,711–27,733, doi:10.1029/96JB01923.

Niu, Y. L., K. D. Collerson, R. Batiza, J. I. Wendt, and M. Regelous (1999), Origin of enriched-type mid-ocean ridge basalt at ridges far from mantle plumes: The East Pacific Rise at 11°20′N, *J. Geophys. Res.*, *104*, 7067–7087, doi:10.1029/1998JB900037.

Nowell, G. M., P. D. Kempton, S. R. Noble, J. G. Fitton, A. D. Saunders, J. J. Mahoney, and R. N. Taylor (1998), High precision Hf isotope measurements of MORB and OIB by thermal ionisation mass spectrometry: Insights into the depleted mantle, *Chem. Geol.*, *149*, 211–233, doi:10.1016/S0009-2541(98)00036-9.

Palacz, Z. A., and A. D. Saunders (1986), Coupled trace element and isotope enrichment in the Cook-Austral-Samoa Island, southern Pacific, *Earth Planet. Sci. Lett.*, *79*, 270–280.

Pearce, J. A., M. Ernewein, S. H. Bloomer, L. M. Parson, B. J. Murton, and L. E. Johnson (1994), Geochemistry of Lau basin volcanic rocks: Influence of ridge segmentation and

arc proximity, *Geol. Soc. Spec. Publ.*, *81*, 53–75, doi:10.1144/GSL.SP.1994.081.01.04.

Pearce, J. A., P. E. Baker, P. K. Harvey, and I. W. Luff (1995), Geochemical evidence for subduction fluxes, mantle melting and fractional crystallization beneath the south Sandwich island arc, *J. Petrol.*, *36*, 1073–1109.

Pearce, J. A., R. J. Stern, S. H. Bloomer, and P. Fryer (2005), Geochemical mapping of the Mariana arc-basin system: Implications for the nature and distribution of subduction components, *Geochem. Geophys. Geosyst.*, *6*, Q07006, doi:10.1029/2004GC000895.

Pearce, J. A., P. D. Kempton, and J. B. Gill (2007), Hf-Nd evidence for the origin and distribution of mantle domains in the SW Pacific, *Earth Planet. Sci. Lett.*, *260*, 98–114, doi:10.1016/j.epsl.2007.05.023.

Peate, D. W., and J. A. Pearce (1998), Causes of spatial compositional variations in Mariana arc lavas: Trace element evidence, *Isl. Arc*, *7*, 479–495, doi:10.1111/j.1440-1738.1998.00205.x.

Peate, D. W., T. F. Kokfelt, C. J. Hawkesworth, P. W. Van Calsteren, J. M. Hergt, and J. A. Pearce (2001), U-series isotope data on Lau basin glasses: The role of subduction-related fluids during melt generation in back-arc basins, *J. Petrol.*, *42*, 1449–1470.

Plank, T. (2005), Constraints from thorium/lanthanum on sediment recycling at subduction zones and the evolution of the continents, *J. Petrol.*, *46*, 921–944, doi:10.1093/petrology/egi005.

Prinzhofer, A., E. Lewin, and C. J. Allègre (1989), Stochastic melting of a marble cake mantle: Evidence from local study of the East Pacific Rise at 12°50′N, *Earth Planet. Sci. Lett.*, *92*, 189–206, doi:10.1016/0012-821X(89)90046-0.

Regelous, M., K. D. Collerson, A. Ewart, and J. I. Wendt (1997), Trace element transport rates in subduction zones: Evidence from Th, Sr and Pb isotope data for Tonga-Kermadec arc lavas, *Earth Planet. Sci. Lett.*, *150*, 291–302, doi:10.1016/S0012-821X(97)00107-6.

Regelous, M., Y. Niu, J. Wendt, R. Batiza, A. Greig, and K. D. Collerson (1999), Variations in the geochemistry of magmatism on the East Pacific Rise at 10°30′N since 800 ka, *Earth Planet. Sci. Lett.*, *168*, 45–63, doi:10.1016/S0012-821X(99)00048-5.

Rehkämper, M., and A. W. Hofmann (1997), Recycled ocean crust and sediment in Indian Ocean MORB, *Earth Planet. Sci. Lett.*, *147*, 93–106, doi:10.1016/S0012-821X(97)00009-5.

Schiano, P., J. L. Birck, and C. J. Allègre (1997), Osmium-strontium-neodymium-lead isotopic covariations in mid-ocean ridge basalt glasses and heterogeneity of the upper mantle, *Earth Planet. Sci. Lett.*, *150*, 363–379, doi:10.1016/S0012-821X(97)00098-8.

Schilling, J. G. (1985), Upper mantle heterogeneities and dynamics, *Nature*, *314*, 62–67, doi:10.1038/314062a0.

Sinton, J. M., and P. Fryer (1987), Mariana Trough lavas from 18°N: Implications for the origin of back arc basin basalts, *J. Geophys. Res.*, *92*, 12,782–12,802, doi:10.1029/JB092iB12p12782.

Sinton, J. M., L. L. Ford, B. Chappell, and M. T. McCulloch (2003), Magma genesis and mantle heterogeneity in the Manus back-arc basin, Papua New Guinea, *J. Petrol.*, *44*, 159–195, doi:10.1093/petrology/44.1.159.

Staudigel, H., K.-H. Park, M. Pringle, J. L. Rubenstone, W. H. F. Smith, and A. Zindler (1991), The longevity of the South Pacific isotopic and thermal anomaly, *Earth Planet. Sci. Lett.*, *102*, 24–44, doi:10.1016/0012-821X(91)90015-A.

Staudigel, H., T. Plank, B. White, and H.-U. Schmincke (1996), Geochemical fluxes during seafloor alteration of the upper oceanic crust: DSDP sites 417–418, in *Subduction Top to Bottom*, *Geophys. Monogr. Ser.*, vol. 96, edited by G. E. Bebout et al., pp. 19–38, AGU, Washington, D. C.

Stoffers, P., et al. (2006), Submarine volcanoes and high-temperature hydrothermal venting on the Tonga arc, southwest Pacific, *Geology*, *34*, 453–456, doi:10.1130/G22227.1.

Sun, S. S. (1980), Lead isotopic study of young volcanic rocks from mid-ocean ridges, ocean islands and island arcs, *Philos. Trans. R. Soc. London, Ser. A*, *297*, 409–445, doi:10.1098/rsta.1980.0224.

Sun, S. S., and W. F. McDonough (1989), Chemical and isotopic systematics of oceanic basalts: Implications for mantle composition and processes, in *Magmatism in the Ocean Basins*, edited by A. D. Saunders and M. J. Norry, *Geol. Soc. Spec. Publ.*, vol. 42, pp. 313–345, doi:10.1144/GSL.SP.1989.042.01.19.

Sunkel, G. (1990), Origin of petrological and geochemical variations of Lau basin lavas (SW Pacific), *Mar. Min.*, *9*, 205–234.

Tanaka, T., et al. (2000), JNdi-1: A neodymium isotopic reference in consistency with LaJolla neodymium, *Chem. Geol.*, *168*, 279–281, doi:10.1016/S0009-2541(00)00198-4.

Taylor, B., and F. Martinez (2003), Back-arc basin basalt systematics, *Earth Planet. Sci. Lett.*, *210*, 481–497, doi:10.1016/S0012-821X(03)00167-5.

Taylor, B., K. Zellmer, F. Martinez, and A. Goodlife (1996), Sea-floor spreading in the Lau back-arc basin, *Earth Planet. Sci. Lett.*, *144*, 35–40.

Todt, W., R. A. Cliff, A. Hanser, and A. W. Hofmann (1996), Evaluation of a ^{202}Pb–^{205}Pb double spike for high-precision lead isotope analysis, in *Earth Processes: Reading the Isotopic Code*, *Geophys. Monogr. Ser.*, vol. 95, edited by S. R. Hart and A. Basu, pp. 429–437, AGU, Washington, D. C.

Turner, S. P., and C. J. Hawkesworth (1997), Constraints on flux rates and mantle dynamics beneath island arcs from Tonga-Kermadec lava geochemistry, *Nature*, *389*, 568–573, doi:10.1038/39257.

Turner, S. P., and C. J. Hawkesworth (1998), Using geochemistry to map mantle flow beneath the Lau basin, *Geology*, *26*, 1019–1022, doi:10.1130/0091-7613(1998)026<1019:UGTMMF>2.3.CO;2.

Turner, S., C. J. Hawkesworth, N. Rogers, J. Bartlett, T. Worthington, J. M. Hergt, J. A. Pearce, and I. Smith (1997), ^{238}U-^{230}Th disequilibria, magma petrogenesis, and flux rates beneath the depleted Tonga-Kermadec island arc, *Geochim. Cosmochim. Acta*, *61*, 4855–4884, doi:10.1016/S0016-7037(97)00281-0.

Vidal, P., and N. Clauer (1981), Pb and Sr isotopic systematics of some basalts and sulfides from the East Pacific Rise at 21°N (Project Rita), *Earth Planet. Sci. Lett.*, *55*, 237–246, doi:10.1016/0012-821X(81)90103-5.

Volpe, A. M., J. D. Macdougall, and J. W. Hawkins (1988), Lau basin basalts (LBB): Trace element and Sr-Nd isotopic evidence for heterogeneity in back-arc basin mantle, *Earth Planet. Sci. Lett.*, *90*, 174–186, doi:10.1016/0012-821X(88)90099-4.

Volpe, A. M., J. D. Macdougall, G. W. Lugmair, J. W. Hawkins, and P. Lonsdale (1990), Fine-scale isotopic variation in Mariana Trough basalts: Evidence for heterogeneity and a recycled component in backarc basin mantle, *Earth Planet. Sci. Lett.*, *100*, 251–264, doi:10.1016/0012-821X(90)90188-4.

Weaver, B. (1991), The origin of ocean island basalt end-member compositions: Trace element and isotopic con-

straint, *Earth Planet. Sci. Lett.*, *104*, 381–397, doi:10.1016/0012-821X(91)90217-6.

Wendt, J. I., M. Regelous, K. D. Collerson, and A. Ewart (1997), Evidence for a contribution from two mantle plumes to island-arc lavas from northern Tonga, *Geology*, *25*, 611–614, doi:10.1130/0091-7613(1997)025<0611:EFACFT>2.3.CO;2.

White, W. M., A. W. Hofmann, and H. Puchelt (1987), Isotope geochemistry of Pacific mid-ocean ridge basalt, *J. Geophys. Res.*, *92*, 4881–4893, doi:10.1029/JB092iB06p04881.

Workman, R. K., and S. R. Hart (2005), Major and trace element composition of the depleted MORB mantle (DMM), *Earth Planet. Sci. Lett.*, *231*, 53–72, doi:10.1016/j.epsl.2004.12.005.

Workman, R. K., S. R. Hart, M. Jackson, M. Regelous, K. A. Farley, J. Blusztajn, M. Kurz, and H. Staudigel (2004), Recycled metasomatized lithosphere as the origin of the Enriched Mantle II (EM2) end-member: Evidence from the Samoan Volcanic Chain, *Geochem. Geophys. Geosyst.*, *5*, Q04008, doi:10.1029/2003GC000623.

Wright, E., and W. M. White (1987), The origin of Samoa: New evidence from Sr, Nd, and Pb isotopes, *Earth Planet. Sci. Lett.*, *81*, 151–162, doi:10.1016/0012-821X(87)90152-X.